




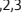


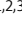

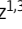
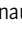


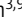

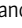



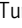

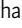

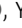
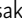





ARTICLE

Encephalitis patient-derived monoclonal GABA_A receptor antibodies cause epileptic seizures

Jakob Kreye^{1,2,3,4,5} , Sukhvir K. Wright^{6,7} , Adriana van Casteren¹ , Laura Stöffler^{1,3} , Marie-Luise Machule^{1,3} , S. Momsen Reincke^{1,2,3,5} , Marc Nikolaus^{4,7,8} , Scott van Hoof^{1,2,3} , Elisa Sanchez-Sendin^{1,2,3} , Marie A. Homeyer^{1,3} , César Cordero Gómez^{1,3} , Hans-Christian Kornau^{1,9} , Dietmar Schmitz^{1,9} , Angela M. Kaindl^{4,8,10} , Philipp Boehm-Sturm^{3,9} , Susanne Mueller^{3,9} , Max A. Wilson⁶ , Manoj A. Upadhy⁶ , Divya R. Dhangar⁶ , Stuart Greenhill⁶ , Gavin Woodhall⁶ , Paul Turko¹¹ , Imre Vida¹¹ , Craig C. Garner¹ , Jonathan Wickel¹² , Christian Geis¹² , Yuko Fukata^{13,14} , Masaki Fukata^{13,14} , and Harald Prüss^{1,2,3} 

Autoantibodies targeting the GABA_A receptor (GABA_AR) hallmark an autoimmune encephalitis presenting with frequent seizures and psychomotor abnormalities. Their pathogenic role is still not well-defined, given the common overlap with further autoantibodies and the lack of patient-derived mAbs. Five GABA_AR mAbs from cerebrospinal fluid cells bound to various epitopes involving the α1 and γ2 receptor subunits, with variable binding strength and partial competition. mAbs selectively reduced GABAergic currents in neuronal cultures without causing receptor internalization. Cerebroventricular infusion of GABA_AR mAbs and Fab fragments into rodents induced a severe phenotype with seizures and increased mortality, reminiscent of encephalitis patients' symptoms. Our results demonstrate direct pathogenicity of autoantibodies on GABA_ARs independent of Fc-mediated effector functions and provide an animal model for GABA_AR encephalitis. They further provide the scientific rationale for clinical treatments using antibody depletion and can serve as tools for the development of antibody-selective immunotherapies.

Introduction

γ-Aminobutyric acid receptors of class A (GABA_ARs) are key molecules for physiological brain function, transmitting rapid phasic inhibitory synaptic signaling and mediating tonic inhibition at extrasynaptic and perisynaptic locations (Farrant and Nusser, 2005). The pentameric ligand-gated chloride channels can be composed of different subunits (α1–6, β1–3, γ1–3, δ, ε, π, θ, and σ1–3), most abundantly in the α1β2γ2 configuration (Olsen and Sieghart, 2008). Receptor dysfunction can lead to severe neurological symptoms, such as epileptic encephalopathies based on GABA_AR subunit mutations (Hernandez et al., 2019; Lachance-Touchette et al., 2010; Maljevic et al., 2006; Wallace et al., 2001). Recently, cerebrospinal fluid (CSF) and serum

autoantibodies targeting the α1-, β3-, and γ2-subunits of GABA_ARs were identified in a new form of autoimmune encephalitis presenting with seizures, refractory status epilepticus, cognitive alterations, psychomotor disorders, and magnetic resonance imaging abnormalities (Ohkawa et al., 2014; Petit-Pedrol et al., 2014; Pettingill et al., 2015; Spatola et al., 2017). Patients' sera or CSF containing polyclonal GABA_AR antibodies caused down-regulation of surface GABA_AR and electrophysiological changes in cultured neurons (Ohkawa et al., 2014; Petit-Pedrol et al., 2014; Pettingill et al., 2015).

Patients with GABA_AR encephalitis frequently harbor further established pathogenic autoantibodies such as those targeting

¹German Center for Neurodegenerative Diseases (DZNE) Berlin, Berlin, Germany; ²Helmholtz Innovation Lab BaoBab (Brain antibody-omics and B-cell Lab), Berlin, Germany; ³Charité-Universitätsmedizin Berlin, corporate member of Freie Universität Berlin and Humboldt-Universität zu Berlin, Department of Neurology and Experimental Neurology, Berlin, Germany; ⁴Charité-Universitätsmedizin Berlin, corporate member of Freie Universität Berlin and Humboldt-Universität zu Berlin, Department of Pediatric Neurology, Berlin, Germany; ⁵Berlin Institute of Health, Berlin, Germany; ⁶Institute of Health and Neurodevelopment, College of Health and Life Sciences, Aston University, Birmingham, UK; ⁷Department of Paediatric Neurology, The Birmingham Women's and Children's Hospital National Health Service Foundation Trust, Birmingham, UK; ⁸Charité-Universitätsmedizin Berlin, corporate member of Freie Universität Berlin and Humboldt-Universität zu Berlin, Center for Chronically Sick Children, Berlin, Germany; ⁹Charité-Universitätsmedizin Berlin, corporate member of Freie Universität Berlin and Humboldt-Universität zu Berlin, Neuroscience Research Center, Cluster NeuroCure, Berlin, Germany; ¹⁰Charité-Universitätsmedizin Berlin, corporate member of Freie Universität Berlin and Humboldt-Universität zu Berlin, Institute of Cell Biology and Neurobiology, Berlin, Germany; ¹¹Charité-Universitätsmedizin Berlin, corporate member of Freie Universität Berlin and Humboldt-Universität zu Berlin, Department of Integrative Neuroanatomy, Berlin, Germany; ¹²Section of Translational Neuroimmunology, Department of Neurology, Jena University Hospital, Jena, Germany; ¹³Division of Membrane Physiology, Department of Molecular and Cellular Physiology, National Institute for Physiological Sciences, National Institutes of Natural Sciences, Okazaki, Japan; ¹⁴Department of Physiological Sciences, School of Life Science, SOKENDAI, The Graduate University for Advanced Studies, Okazaki, Japan.

Correspondence to Jakob Kreye: jakob.kreye@dzne.de; Harald Prüss: harald.pruss@dzne.de.

© 2021 Kreye et al. This article is distributed under the terms of an Attribution–Noncommercial–Share Alike–No Mirror Sites license for the first six months after the publication date (see <http://www.rupress.org/terms/>). After six months it is available under a Creative Commons License (Attribution–Noncommercial–Share Alike 4.0 International license, as described at <https://creativecommons.org/licenses/by-nc-sa/4.0/>).

Leucine-rich, glioma inactivated 1 (LGI1), Contactin associated protein 1 (CASPR2), and N-methyl-D-aspartate receptor (NMDAR; Ohkawa et al., 2014; Petit-Pedrol et al., 2014; Pettingill et al., 2015); hence, it is unclear whether the observed effects exclusively relate to GABA_AR antibodies. Interestingly, in a subset of patients, antibodies against intracellular glutamic acid decarboxylase 65 (GAD65) were observed (Petit-Pedrol et al., 2014), and recently, strongly expanded CD8⁺ T cell clones have been described (Bracher et al., 2020), both pointing toward an accompanying T cell-driven immune response.

In this current study, we aimed to characterize the intrathecal human mAb repertoire from antibody-secreting cells (ASCs) and B cells from CSF in acute GABA_AR encephalitis. Using recombinant production of CSF-derived mAbs (Kornau et al., 2020; Kreye et al., 2016), we generated a set of GABA_AR mAbs for the characterization of antibody sequence features, epitope mapping, and pathogenic functional effects in vitro and in vivo, independent of confounding factors.

Results

Monoclonal CSF antibodies from an encephalitis patient target GABA_AR and non-GABA_AR antigens

To investigate the functional role of GABA_AR antibodies in encephalitis pathogenesis, we first explored the monoclonal Ig repertoire in the CSF of a pediatric GABA_AR encephalitis patient presenting with catatonia (Nikolaus et al., 2018). The antibody response was captured from single cells of three populations: CD138⁺ ASCs, CD20⁺CD27⁺ memory B cells (MBCs), and CD20⁺CD27⁻ nonmemory B cells (NMBCs), separated via fluorescence-activated cell sorting (Fig. S1 A). Using single-cell cloning (Kreye et al., 2020; Kreye et al., 2016), we generated 67 recombinant human mAbs, which were screened for GABA_AR reactivity on cell-based assays (CBAs) and on unfixed murine whole brain sections as an unbiased test for central nervous system (CNS) auto-reactivity.

We identified five different human GABA_AR mAbs. Four reacted positive in two CBAs using human embryonic kidney (HEK) cells expressing either $\alpha 1\beta 3$ (comparable to clinical routine assays) or $\alpha 1\beta 3\gamma 2$ GABA_ARs (Fig. S1 B). In contrast, mAb #113-175 bound to GABA_ARs on the $\alpha 1\beta 3\gamma 2$ CBA only (Fig. S1 B). All five mAbs revealed strong tissue reactivity on murine brain sections (Fig. 1, A–C; and Fig. S3, A–D), most prominently against hippocampal neuropil (Fig. 1, A and B), the granule cell and molecular layer in the cerebellum, putamen, and olfactory bulb. Reactivity to the extracellular domain of GABA_AR was confirmed on cultured live rat neurons (Fig. 1 C) and showed a clustered distribution of GABA_ARs along Microtubule-associated protein 2 (MAP2)-positive dendrites (Fig. 1 D), overlapping with a commercial rabbit GABA_AR- $\alpha 1$ antibody and colocalizing with presynaptic vesicular GABA transporter (VGAT; Fig. 1 E). In addition to a typical neuronal GABA_AR-binding pattern, #113-201 revealed intense reactivity against choroid plexus and around blood vessels (Fig. S2, C and E), in locations where no $\beta 1$ -, $\beta 2$ -, or $\beta 3$ -subunits could be detected (Fig. S2, F–H). β -subunits are essential for functional GABA_AR, thus indicating an additional target for #113-201 independent of GABA_AR. #113-201 (and all other GABA_AR mAbs) did not bind to established polyreactivity-

defining antigens (Fig. S1, J–O), suggesting that this additional reactivity is specific to a distinct target rather than a feature of unspecific binding to a broad variety of antigens.

17 of the expressed GABA_AR-negative mAbs (27.9%) showed intense tissue binding on unfixed murine brain sections in distinct patterns, mostly on neuronal surfaces of the hippocampus, the cerebellum, and in basal ganglia, but others also against blood vessels, choroid plexus, ependyma, and white matter tracts (Fig. 1, F–J; and Fig. S2, I–P). A subset also reacted with fixed cultured neurons (Fig. 1, H–J, inserts). Screening for already established neuronal antigens with commercial assays identified Homer-3 as the target of #113-212 (Fig. 1 J), while the other non-GABA_AR antigens remained unknown.

Polyclonal response to GABA_ARs derived mainly from IgG1 antibody-secreting cells

We next investigated sequence features of the GABA_AR encephalitis Ig repertoire. mAbs derived from different cell populations revealed characteristic Ig isotype distributions (Fig. S1 C and Table S1). All GABA_AR mAbs were of the IgG1 subtype (Fig. S1 D) and derived predominantly from ASCs, also from one MBC, but not from NMBCs (Fig. S1 E). In contrast, CNS tissue-reactive, but GABA_AR-negative mAbs were similarly distributed within different cell populations (Table S1). Among all mAb sequences, no clonal relationships were identified, indicating a polyclonal response to GABA_ARs. Compatible with affinity maturation well known from B cells in other compartments, CSF-derived mAbs from MBCs carried more somatic hypermutations (SHMs) than mAbs from NMBCs on heavy chains, light chains, and per mAb in total (22.6 ± 12.8 vs. 10.1 ± 8.6 ; $P = 0.0001$, ANOVA, post hoc Tukey's multiple comparisons test; Fig. S1 F and Table S1). SHM counts of ASC mAbs (14.2 ± 1.9) were between those of MBC and NMBC mAbs (Fig. S1 F). GABA_AR mAbs contained a similar number of SHMs as GABA_AR-negative mAbs (Fig. S1 G). Within GABA_AR mAbs, SHMs were higher in frequency and replacement to silence ratios in complementarity-determining regions (CDRs) than in frame regions (FRs; Fig. S1, H and I), characteristic of antigen-driven maturation.

Patient-derived mAbs bound $\alpha 1$ - and $\gamma 2$ -subunits of GABA_AR with different strengths and partial competition

To select the most relevant antibodies for functional studies, we aimed to characterize the subunit specificity and the binding strength of the isolated GABA_ARs mAbs. To this end, we first performed a series of CBAs expressing individual rodent GABA_AR subunits or combinations thereof. The patient samples of CSF and plasmapheresis eluate (PPE) containing polyclonal antibodies showed predominantly an $\alpha 1$ reactivity. Additionally, they bound very weakly to cells expressing subunit combinations of $\alpha 2\beta 3$, $\alpha 5\beta 3$ (CSF and PPE), and $\beta 3\gamma 2$ (PPE only; Fig. 2 A and Fig. S3 A). mAb stainings confirmed the $\alpha 1$ subunit as the main immunogenic target of the GABA_AR (Fig. 2 A and Fig. S3 A) and excluded binding to $\alpha 1$ -5-, $\beta 1$ -3-, or $\gamma 2$ -subunits for all further mAbs with anti-neuronal reactivity (Fig. 2 A, exemplarily shown for #113-109). Whereas GABA_AR mAbs #113-101, #113-115, and #113-198 selectively target $\alpha 1$, #113-201 additionally bound $\gamma 2$ as an independent target (Fig. 2 A). GABA_AR reactivity of #113-175 is also $\alpha 1$ and

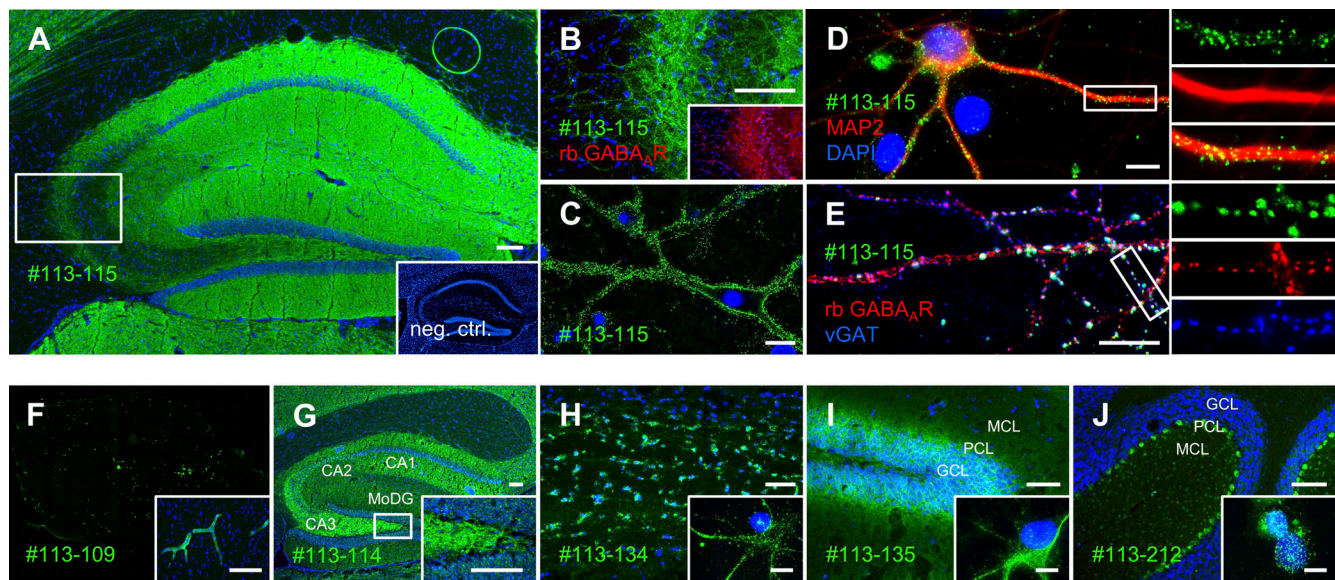


Figure 1. Binding of human mAbs to GABA_AR and other CNS targets. (A and B) Immunofluorescence stainings of human GABA_AR mAb #113-115 (green) on unfixed murine brain tissue, with binding to hippocampal neuropil. (B) Higher magnification of the hippocampal CA3 area showing the colocalization with a commercial anti-GABA_AR antibody (red; nuclei in blue). (C) Live-cell staining of GABA_AR mAb #113-115 on cultured cortical rat neurons. (D and E) Immunofluorescence staining on fixed cultured cortical rat neurons, with GABA_AR mAb #113-115 (green) in D with clustered binding pattern along MAP2⁺ (red) dendrites and in E colocalization with commercial antibodies against GABA_AR (red) and the presynaptic marker vGAT (blue). (F–J) Immunofluorescence staining of human GABA_AR-negative mAbs (green; nuclei in blue) from encephalitis patient’s CSF repertoire with reactivity in variable distribution patterns on unfixed murine brain sections, including binding to blood vessels (F), hippocampal neuropil (G), cell soma in corpus callosum (H), and cells of different cerebellar layers (J and I). F shows a tile scan of a whole sagittal brain section. Inserts in H–J show mAb staining on fixed cultured neurons. All stainings were replicated at least twice on tissue or neurons from two different animals. Scale bars indicate 100 μm in A and B, 20 μm in C–E, 100 μm in F–J, and 20 μm in inserts of F–J. GCL, granule cell layer; MCL, molecular cell layer; MoDG, molecular layer of the dentate gyrus; neg. ctrl, negative control; PCL, Purkinje cell layer; rb, rabbit.

γ2 mediated but requires their coexpression (Fig. 2 A and Fig. S3 A), suggesting that #113-175 recognizes a three-dimensional epitope of α1γ2-containing GABA_AR heteromers.

For the identification of the mAb with the strongest binding to natively expressed GABA_ARs, we then quantified binding of purified mAbs at serial dilutions to murine cerebellum (Fig. 2 B). Binding curves were derived from mean fluorescence intensities (MFIs) to quantify maximum intensity (MFI_{max}) and concentrations at which 50% of MFI_{max} is reached (Half Max; Table S2). #113-115 showed strongest reactivity (Fig. 2 B, red), as indicated by lowest Half Max of 160 ng/ml, which was ~40-fold higher than that of the weakest binder #113-201 (Fig. 2 B, orange). Models from four out of five mAbs displayed similar MFI_{max}. This indicates likewise similar available binding sites, which for α1-selective mAbs are represented by the presence of two α1-subunits and therefore two binding sites per heteropentameric GABA_AR. In contrast, the target epitope of #113-175 involves the α1- and γ2-subunit and therefore can likely be present only once per GABA_AR. Consistently, mAb #113-175 reached a considerably lower MFI_{max}, but with a similar concentration dependency as #113-115 (Fig. 2 B, purple). In a complementary assay using flow cytometry, we found similar binding to HEK cells over-expressing rat α1β3γ2 GABA_AR for all five mAbs (Fig. S3, B–D and F; and Table S2). In contrast, when using HEK cells over-expressing human α1β3γ2 GABA_AR, Half Max values were similar for four out of five mAbs only and were ~200-fold lower for #113-201 (Fig. S3, E and G; and Table S2), indicating preferential binding to the human receptor.

As GABA_AR binding for all mAbs involves α1, we analyzed whether target epitopes are identical or in close proximity in a competition assay. GABA_AR mAbs were fluorophore-coupled and used for quantitative detection of binding to murine cerebellum. The binding of each fluorophore-coupled GABA_AR mAb was abrogated in the presence of its respective unlabeled mAb at excess, but not when coapplied with nonreactive control mAb #mGO53 (Fig. 2 C). Quantification of all possible pairings of GABA_AR mAbs revealed that certain mAbs can decrease the binding of other GABA_AR mAbs (Fig. 2 C, black tiles), suggesting competition for overlapping target epitopes. In contrast, #113-201 did not influence receptor binding of any other GABA_AR mAb. Interestingly, the binding signal of #113-101 was markedly increased in the presence of unlabeled #113-115 (Fig. 2 C, yellow tile) and similarly with #113-115 fragment antigen-binding (Fab) fragments (Fig. S3 H). As #113-101 did not directly bind #113-115 (Fig. S3, I and J), this finding suggests conformational GABA_AR changes induced by #113-115 binding, leading to increased #113-101 epitope accessibility in vitro.

mAb #113-115 selectively reduced GABAergic currents without causing receptor internalization

Next, we explored the pathogenic relevance of single GABA_AR mAbs on GABAergic functions in vitro. We selected #113-115, being the mAb with strongest binding to native GABA_ARs, and #113-175, which depends on α1γ2 coexpression. In electrophysiological recordings from cultured autaptic neurons incubated for 24 h with 1 μg/ml of #113-175, we observed no differences

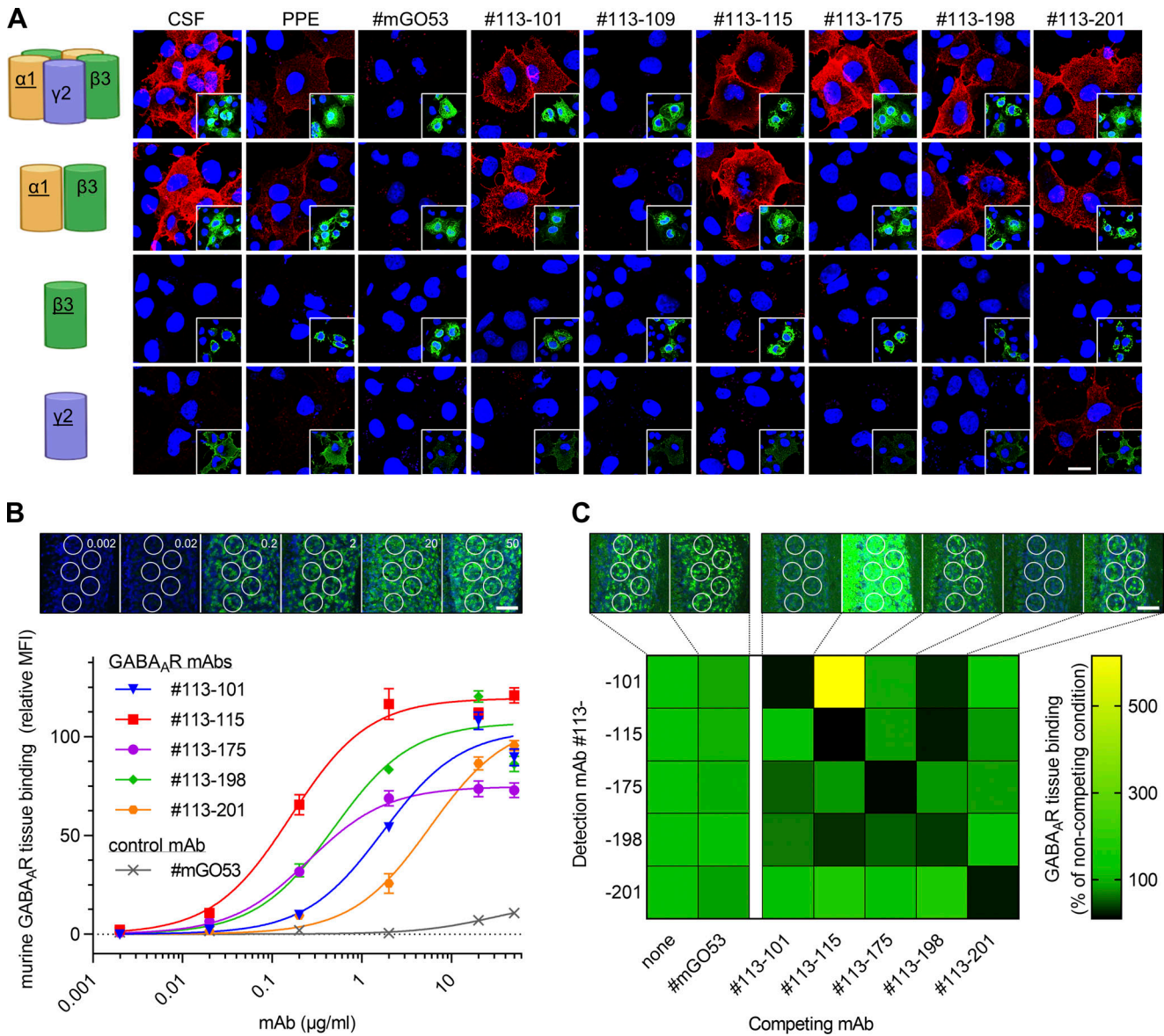


Figure 2. GABA_AR subunit epitopes and mAb binding properties. (A) Immunofluorescence stainings as CBAs using COS7 cells overexpressing individual or multiple GABA_AR subunits (as illustrated in left column) to evaluate subunit-specific binding of patient’s polyclonal samples and derived recombinant mAbs (red; nuclei in blue). Negative controls #mGO53 and #113-109 showed no binding. Underlined subunits were stained with subunit-specific commercial antibodies (shown in green in image inserts). Note that β3 alone is expressed on the cell surface, but α1 alone is not (Ebert et al., 1999). (B) For relative quantification of human GABA_AR mAb binding to natively expressed receptors, the MFI was measured from binding in the granule cell layer of the murine cerebellum. Representative images from #113-115 are shown in top row with IgG concentrations as indicated. Per condition, MFIs from 15 ROIs from three independent experiments were used to fit nonlinear regression models of specific binding. Bars indicate mean ± SEM. (C) For analysis of competitive binding, fluorophore-coupled GABA_AR mAbs (detection mAbs) were stained on murine brain tissue in combination with an uncoupled mAb (competing mAb) in excess. The degree of detection mAb labeling was between 7.2 (#113-115) and 17.5 (#113-198). Exemplary images from coupled #113-101 are shown in top row. Quantified mean MFIs as relative values to noncompeting condition of the respective coupled mAb are shown as a heat map, each derived from 45 ROIs from three independent experiments. Receptor binding competition is visualized in black and signal enhancement in yellow. Representative scale bars indicate 20 μm in A and 100 μm in B and C.

with untreated and control conditions. In contrast, #113-115 led to reduced inhibitory postsynaptic signaling, as indicated in lower amplitudes of evoked inhibitory postsynaptic currents (IPSCs; Fig. 3, A and C), in comparison with untreated condition and with control mAb treatment (#113-115: 0.31 ± 0.09 SEM; untreated: 1 ± 0.12, P < 0.0001, Kruskal-Wallis, Dunn’s post hoc; control: 0.91 ± 0.16, P = 0.0037). This effect

was GABA specific, as amplitudes of selective responses to GABA (Fig. 3, B and D) were likewise reduced (#113-115: 0.55 ± 0.06; untreated: 1 ± 0.09, P = 0.0011; control: 1.02 ± 0.07, P = 0.0001), whereas responses to kainate and NMDA remained unaffected (Fig. 3, E and F).

Previous studies using patients’ sera or CSF containing GABA_AR antibodies suggested receptor internalization as a

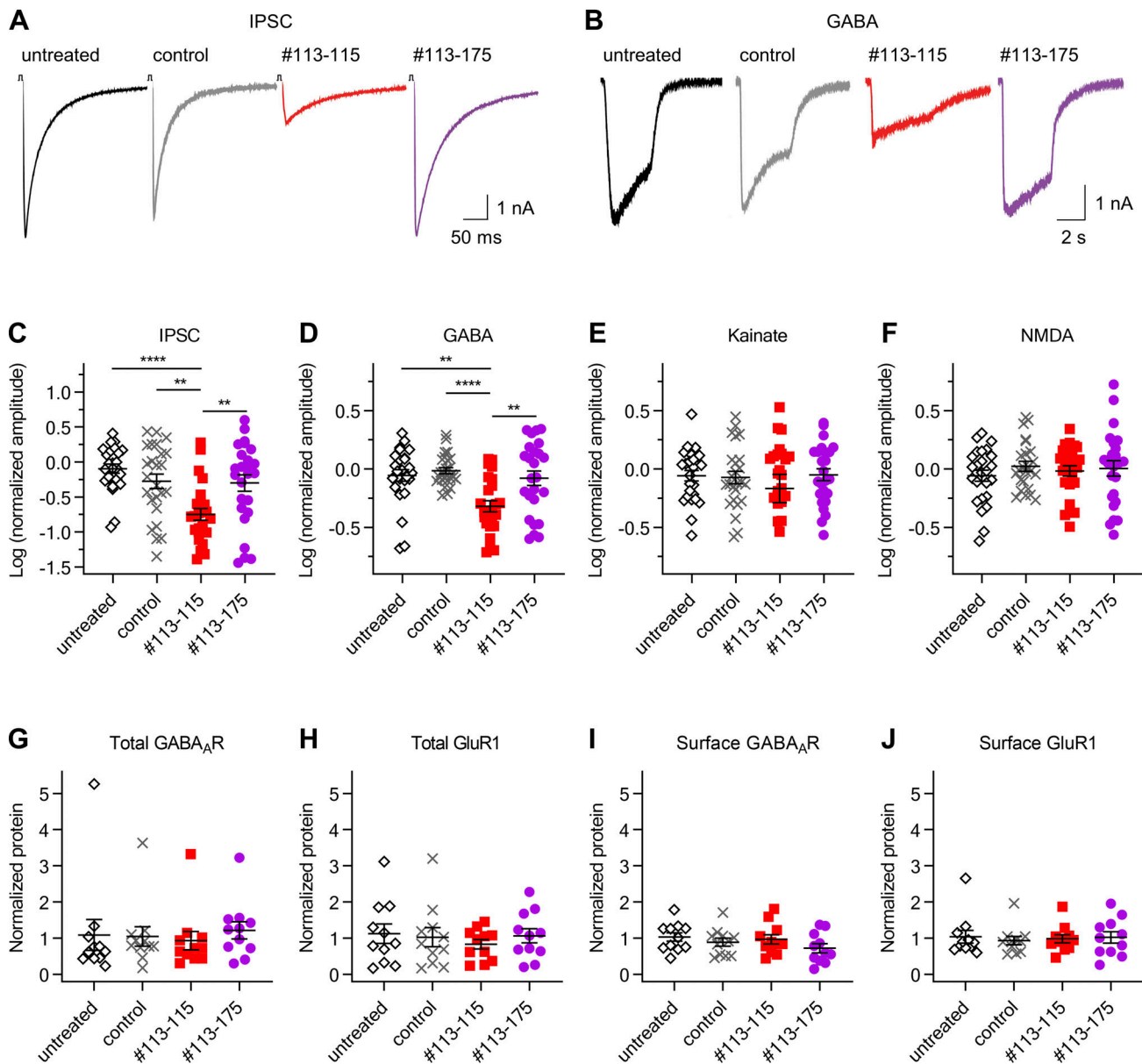


Figure 3. mAb #113-115 selectively reduced GABAergic signaling in vitro, independent of receptor internalization. (A and B) Representative traces from evoked (A) or GABA-dependent (B) currents of murine autaptic neurons after preincubation with indicated human mAb. **(C–F)** Amplitudes of evoked or chemically induced responses (C) to GABA (D), kainite (E), or NMDA (F) of murine autaptic neurons after mAb preincubation as indicated (values normalized to mean of untreated condition). Data were analyzed using Kruskal-Wallis, Dunn’s post hoc tests (**, $P \leq 0.01$; ****, $P \leq 0.0001$; or not shown when $P > 0.05$). Each dot represents one neuron, $n = 25$ per condition. Bars indicate mean \pm SEM. **(G–J)** Quantifications of the indicated total (G and H) and biotinylated surface (I and J) proteins from cultured neocortical rat neurons as analyzed by Western blotting (values normalized to N-Cadherin expression and mean of untreated condition). Each dot represents one preparation after mAb treatment, $n = 11$ per condition from four separate neuronal cultures. Bars indicate mean \pm SEM.

pathogenic mechanism in GABA_AR encephalitis. To examine this mechanism at the level of mAbs, we quantified protein levels from neuronal cultures after mAb incubation (Fig. S4, A–C; and Fig. 3, G–J). The expression levels of GABA_AR and control protein glutamate receptor 1 (GluR1) were unaltered under mAb treatment and control conditions, both in the total protein (Fig. 3, G and H) and in the surface protein fractions (Fig. 3, I and J). Control experiments ensured the presence and stability of mAbs after the culture conditions (Fig. S4, D and E). These results were independently confirmed using reader-based immunocytochemistry to

quantify surface GABA_AR levels of neuronal cultures, which displayed no changes between all groups (Fig. S4 F).

Cerebroventricular infusion of #113-115 IgG and Fab fragments induced encephalopathic symptoms and increased mortality

The effects observed in vitro indicate direct pathogenicity of antibody–antigen binding, independent of receptor internalization, a mechanism related to bivalent antibody-mediated cross-linking (Hughes et al., 2010). To explore the role of the antibody’s bivalence for its functionality, we generated and characterized a

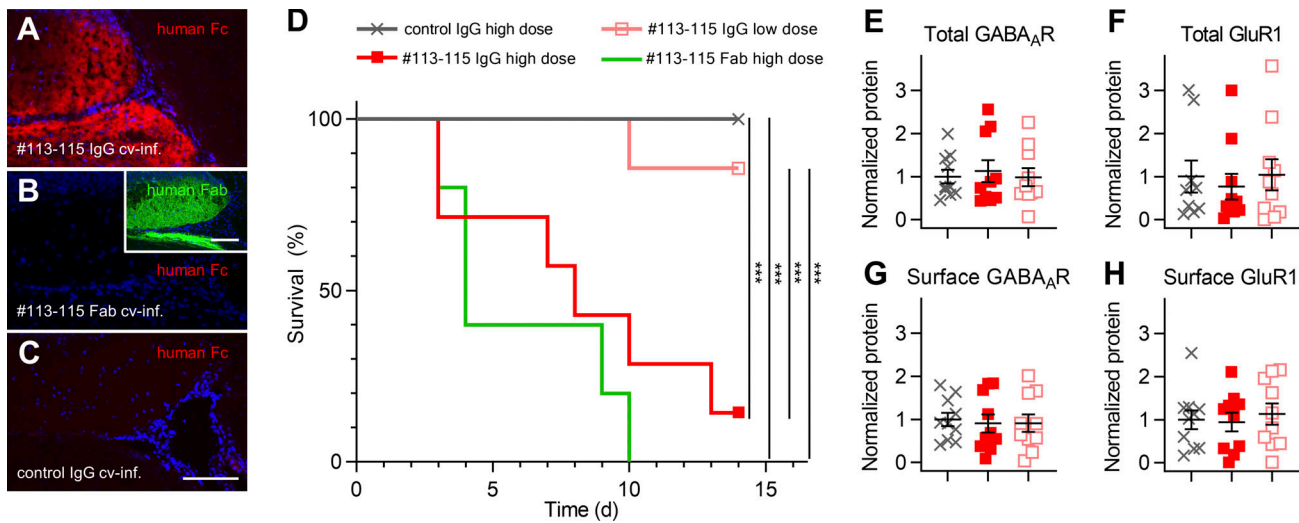


Figure 4. GABA_AR IgG- and Fab-induced increased mortality. (A–C) Immunofluorescence stainings on brain sections from C57BL/6 mice after cerebroventricular infusion (cv-inf.) of the indicated GABA_AR or control mAbs over 14 d. Detection with anti-human Fc-specific antibody (red) or anti-human Fab-specific antibody (green; insert in B) revealed characteristic hippocampal mAb deposition of #113-115 IgG (A) and #113-115 Fab (B). (C) Not seen in control animals receiving control IgG (#mGO53). Representative scale bars indicate 100 μm. (D) Kaplan-Meier plot for survival of C57BL/6 mice after cerebroventricular infusion over 14 d of indicated mAbs as IgG in high or low dose (1.5/0.3 μg IgG per hour) or as Fab in high dose. Survival was significantly different as analyzed using log-rank Mantel-Cox ($P \leq 0.0001$), followed by ANOVA, post hoc Tukey’s multiple comparisons (***, $P \leq 0.001$; or not shown when $P > 0.05$; $n = 5–7$ animals per group). (E–H) Quantifications of the indicated total (E and F) and surface (G and H) proteins from murine brain homogenates after cerebroventricular mAb infusion as analyzed by Western blotting and normalized to mean of control IgG group. Each dot represents one hemisphere, $n = 10$ per condition. Bars indicate mean \pm SEM.

monovalent Fab fragment version of #113-115 lacking the fragment crystallizable (Fc) domain (Fig. S5, A and B). Next, we used the #113-115 IgG and Fab to assess whether they can similarly induce pathogenic effects in vivo when applied in mice by continuous cerebroventricular infusion via osmotic pumps.

Within a few days after implantation, six out of seven mice of the #113-115 IgG high-dose (1.5 μg of IgG per hour) group and all five mice of the #113-115 Fab high-dose group developed encephalopathic symptoms compatible with impaired GABAergic inhibition, including myoclonus, twitching, gait ataxia, and circling (Video 1 and Table S3). In the #113-115 IgG low-dose group (0.3 μg per hour) only two out of six mice developed similar symptoms, which started later after pump implantation. No disease symptoms were observed in the control mice after mAb #mGO53 infusion. All symptomatic mice in the #113-115 IgG high-dose and #113-115 Fab group died or had to be sacrificed after reaching predefined humane endpoints, commonly status epilepticus (Fig. 4 D and Table S3).

Extracted brains from #113-115-infused but not #mGO53-infused mice revealed intense deposition of human IgG or Fab in a characteristic GABA_AR distribution pattern (Fig. 4, A–C), indicating in vivo antigen binding. However, the levels of GABA_AR and control proteins from homogenized extracted brains showed no differences between the groups (Fig. 4, E–H), consistent with the in vitro data (Fig. 3, G–J; and Fig. S4 F).

GABA_AR mAbs caused spontaneous seizures in vivo and spontaneous epileptic activity ex vivo

The mAb-induced in vivo phenotype suggested hyperexcitability and seizures. We used a wireless electroencephalography

(EEG) system to further evaluate the influence of GABA_AR mAbs on electric activity at lower concentrations not causing mortality. We examined 15 male Wistar P21 rats that received cerebroventricular infusion of GABA_AR mAbs or controls over 7 d and were concurrently implanted with EEG transmitters to record ictal events (Fig. 5 A). The EEG coastline length was significantly higher in the GABA_AR mAb-infused animals, indicating increased epileptiform activity (Fig. 5 B). For the application of #113-115 and also of α1γ2-dependent #113-175, this correlated with an increase of ictal events as detected by the automated seizure detection program (Fig. 5, C and D), including Racine stage 5 seizures (Fig. S5 C and Video 2; Lüttjohann et al., 2009). In a subgroup of three GABA_AR mAb-infused animals, we performed prolonged EEG recordings over 21 d. Ictal events were detected until the end of the recording period, although at a lower level than during the infusion (Fig. S5 D), correlating also with a peak in the postseizure behavioral battery (PSBB) score, indicating the animals’ hyperexcitability and aggression (Fig. S5 E). The EEG of the GABA_AR mAb animals showed significantly higher power in all the power band ranges (Fig. 5 E).

After the completion of infusion with GABA_AR or control mAbs (days 7–8), acute sagittal brain slices were prepared for local field potential recordings to assess for spontaneous epileptic activity from electrodes placed in areas CA3 and CA1 of the hippocampus. There were significantly higher numbers of spontaneous epileptic events during recordings from the GABA_AR mAb-infused animals at day 7/8 and at day 21 compared with controls from day 7/8 (Fig. 5, F and G). This shows a preservation of the prolonged epileptic activity seen in vivo from depth electrode recordings of the GABA_AR mAb-infused animals.

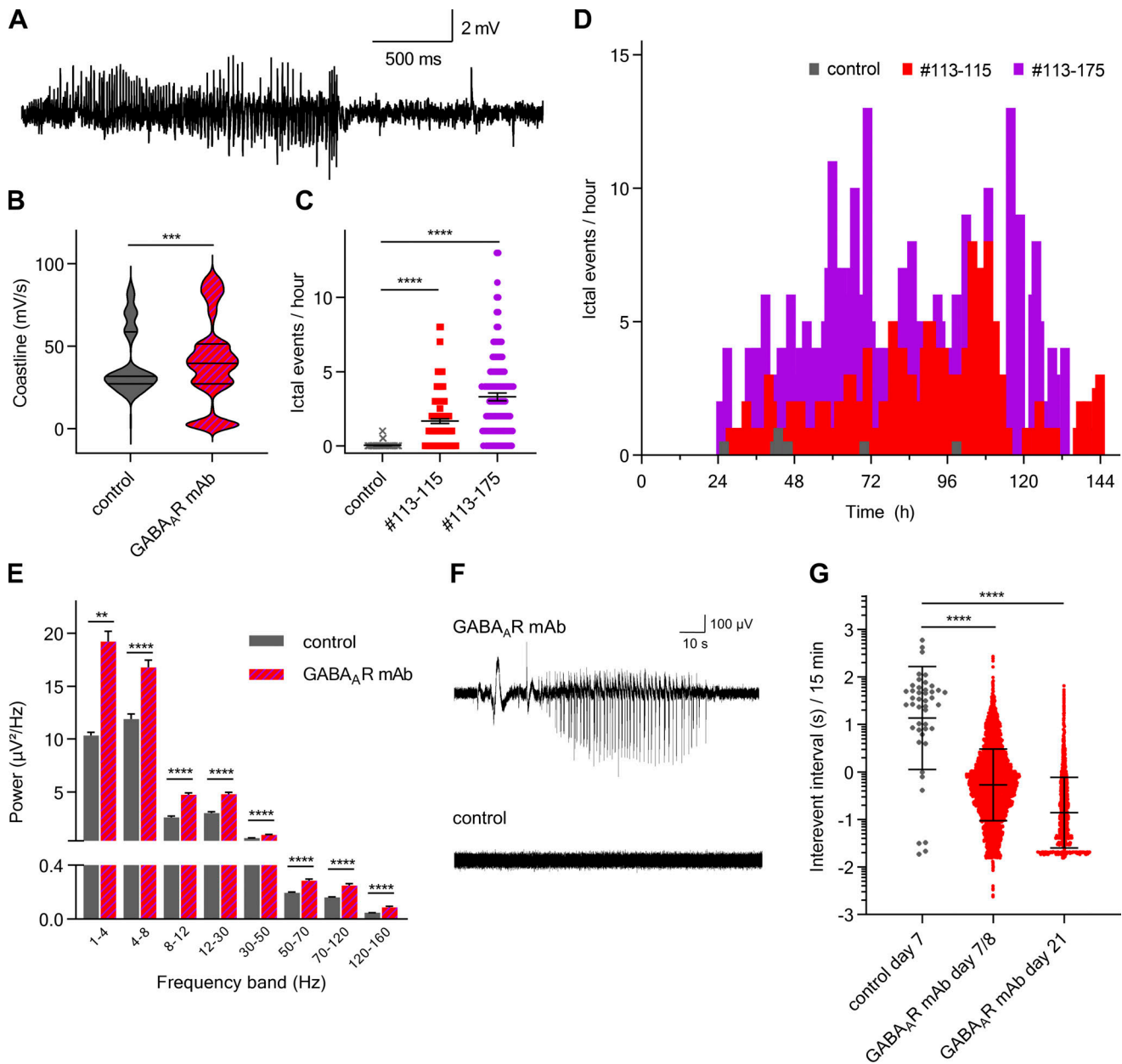


Figure 5. **GABA_AR mAbs caused spontaneous seizures in vivo and spontaneous epileptic activity ex vivo.** (A) Representative EEG of an ictal event recorded from a CA3 depth electrode in a Wistar rat receiving GABA_AR mAb infusion. (B) Comparison of hourly averages of coastline length between GABA_AR mAb (#113-115, *n* = 3; #113-175, *n* = 3) and control (*n* = 6) infused animals, analyzed using Mann-Whitney (***, *P* ≤ 0.001; *n* = 900–905 average values per group). Horizontal lines indicate mean and quartiles. (C) Comparison of the hourly ictal event counts between animals during infusion with GABA_AR mAb or control as analyzed from Neuroarchiver seizure detection software and using Mann-Whitney (****, *P* ≤ 0.0001). Animal numbers as in B, *n* = 120 events per group. Bars indicate mean ± SEM. (D) Distribution of the detected ictal event over time. (E) Comparison of hourly EEG power averages throughout 7-d recordings during GABA_AR mAb or control infusion, analyzed using Mann-Whitney (**, *P* ≤ 0.01; ****, *P* ≤ 0.0001). Animal numbers as in B, *n* = 899–900 average values per group. Bars indicate mean + SEM. (F) Local field potential recording from the CA3 region in a sagittal brain slice from a rat after GABA_AR mAb infusion (upper trace) showing spontaneous ictal activity ex vivo, not seen in controls (lower trace). (G) Comparison of interevent intervals of spontaneous ictal activity from postmortem acute brain slice recordings from rats after cerebroventricular antibody infusion over 7 d. Recordings from GABA_AR mAb-exposed brains are from day 7/8 (#113-115, *n* = 3; #113-175, *n* = 3) or day 21 after beginning of infusion and from day 7 of control exposed brains (*n* = 6), analyzed using Mann-Whitney (****, *P* ≤ 0.0001; *n* = 44–10,302 intervals per group). Bars indicate geometric mean ± SD.

Discussion

Here, we provide insight into the CSF antibody repertoire of acute GABA_AR encephalitis. So far, only a few studies have investigated patient-derived mAbs from different forms of autoantibody-mediated encephalitis. These reports included

either only a single target-specific mAb (Brändle et al., 2021; Malviya et al., 2017) or only mAbs that were isolated from the periphery (Ramberger et al., 2020; Sharma et al., 2018) and also did not observe a phenotype mimicking the patients' key symptoms (Malviya et al., 2017; Ramberger et al., 2020; Sharma

et al., 2018) or completely lacked in vivo data (Brändle et al., 2021; Kornau et al., 2020; Kreye et al., 2016). In contrast, we here present a systematic characterization of the functional role of patient-derived disease-specific anti-neuronal autoantibodies in GABA_AR encephalitis. Using a recombinant single-cell cloning approach, we isolated five monoclonal human GABA_AR autoantibodies and comprehensively showed that they recognized GABA_ARs in vitro and in vivo, induced electrophysiological effects independent of receptor internalization, and caused a severe encephalitic phenotype in two rodent models. Unlike human serum or CSF containing polyclonal autoantibodies against GABA_AR and potentially other targets, the mAbs allowed the detailed analysis of antibody sequences, epitope mapping, and autoantibody-specific pathogenic functional effects, resulting in a number of novel findings.

The identified GABA_AR mAbs revealed typical indicators of affinity maturation, similar to LGII mAbs (Kornau et al., 2020; Ramberger et al., 2020) and in contrast to NMDAR mAbs that we and others have reported with low SHM numbers (Kreye et al., 2016; Malviya et al., 2017) or even in germline configuration (Wenke et al., 2019). The main epitope of all five GABA_AR mAbs was the $\alpha 1$ receptor subunit, as suggested from previous studies using polyclonal patient samples (Petit-Pedrol et al., 2014; Pettingill et al., 2015) and by one mAb that has recently been reported (Brändle et al., 2021). However, in our study one mAb independently codetected the $\gamma 2$ -subunit, and another bound to a shared epitope requiring both $\alpha 1$ and $\gamma 2$ receptor subunits. Importantly, the latter mAb therefore cannot be detected in current commercial CBAs that use $\alpha 1\beta 3$ GABA_AR, with the potential implication that routine diagnostics in acute encephalitis may underestimate disease-relevant GABA_AR antibody titers or even overlook affected patients, in case patients harbor only antibodies directed to $\gamma 2$ receptor subunits in their polyclonal antibody response. The target epitopes of some GABA_AR mAbs were identical or in close proximity, as shown in our antibody competition assays and indicated from prior experiments with the limitations of CSF polyclonality (Petit-Pedrol et al., 2014). Conversely, the presence of mAb #113-115 did not reduce but enhanced binding of mAb #113-101 to the GABA_AR. This suggests a direct conformational change of the receptor upon mAb binding, thus potentially adding a new pathogenic principle to the complexity of antibody-induced effects in autoimmune encephalitis. Likewise, conformational effects of disease-relevant mAbs may in some cases stabilize the receptor in a specific activation state, similar to nanobodies that, in this way, allowed first structure crystallography of G protein-coupled receptors complexed with their G protein (Rasmussen et al., 2011).

Our functional investigations in vitro and in vivo showed the pathogenicity of the two selected GABA_AR mAbs #113-115 and $\alpha 1\gamma 2$ -dependent #113-175. Cerebroventricular infusion of both mAbs induced a severe phenotype with seizures and increased mortality, similar to encephalitis patients and in line with epileptic encephalopathies in GABA_AR mutation carriers (Hernandez et al., 2019; Lachance-Touchette et al., 2010; Maljevic et al., 2006; Wallace et al., 2001). However, electrophysiological recordings from autaptic neuronal cultures revealed a reduction of GABAergic currents for mAb #113-115, but not for $\alpha 1\gamma 2$ -dependent

#113-175. The observed increase of epileptiform activity in vivo after #113-175 infusion may, among other reasons, be mediated via yet unknown factor(s) that are not present in vitro, via receptor modulation (e.g., by affecting the access of benzodiazepine-like compounds) or via network effects, and thus may not be detectable in all cases in the autaptic in vitro model. For both mAbs, we did not observe receptor internalization, a previously highlighted mechanism (Ohkawa et al., 2014; Pettingill et al., 2015). Possible explanations for the different findings include the use of patient samples containing polyclonal antibodies with undetermined additional specificities in previous studies and the presence of GABA_AR $\beta 3$ -subunit antibodies not assessed in our study. For #113-115, the electrophysiological findings and missing internalization together with the suggested change of receptor conformation indicate direct functional effects upon mAb binding. Possible mechanisms include stabilization of the receptor in a desensitized state similar to the GABA_AR agonist benzamidine (Miller and Aricescu, 2014), allosteric modulation of the physiological GABA-binding affinity and/or neurotransmission efficacy, and orthosteric GABA antagonism. Additionally, redistribution of GABA_AR between synaptic and extrasynaptic locations may further contribute to GABAergic dysfunction, as likewise reported from NMDAR autoantibodies (Jézéquel et al., 2017; Ladépêche et al., 2018). Pathogenic mechanisms beyond internalization alone had been suggested by previous results (Ohkawa et al., 2014), showing a frequency reduction of IPSCs after GABA_AR antibody application. Furthermore, our additional in vivo experiments using monovalent GABA_AR Fab fragments not only replicated the severe mAb-induced phenotype but also supported the concept of direct effects of autoantibody-autoantigen binding, similar to recent studies in which polyclonal Fab fragment preparations of glycine receptor autoantibodies specifically reduced glycinergic currents (Crisp et al., 2019). In both cases, Fab fragment experiments prove mAb pathogenicity independent of the integrity of the whole antibody, thereby excluding the dependency of the antibody's bivalence and Fc-mediated effector functions such as antibody-dependent cell-mediated cytotoxicity, antibody-dependent cellular phagocytosis, and complement-dependent cytotoxicity.

GABA_AR encephalitis leads to frequent seizures, including epilepsy partialis continua and treatment-refractory status epilepticus (Petit-Pedrol et al., 2014; Spatola et al., 2017), which was the predominant phenotype also in our animal models. Future studies should compare whether the intrathecal application into rodents of polyclonal CSF from patients of a larger cohort induces similar effects. Here, using wireless EEG in living animals, we could quantify epileptiform activity. Ictal events peaked under the mAb delivery and remained until the end of the recording period, 14 d after termination of the infusion. Such persistence has not been observed in NMDAR encephalitis models, where cognitive changes were reversible after 10 d (Malviya et al., 2017; Planagumà et al., 2015). Extended measures revealed higher coastline length (Jones and Heinemann, 1988) and increased power in the lower frequency range (1–4 Hz), consistent with EEG changes in human encephalitis patients (Symmonds et al., 2018). Interestingly, in a pharmacologically induced rodent model of status epilepticus, spontaneous seizures were also associated with increased γ , θ , and Δ powers in

the power spectrum, similar to our GABA_AR mAb model (Puttachary et al., 2015).

Similar to our findings in the related NMDAR encephalitis (Kreye et al., 2016), we found a broad spectrum of CNS auto-reactivity beyond GABA_ARs. These mAbs were reactive to surface and intracellular epitopes on neurons, endothelium, and choroid plexus. For example, we identified one anti-Homer-3 antibody, a known target protein in some patients with autoimmune cerebellitis and ataxia (Höftberger et al., 2013). Ongoing attempts to identify other auto-antigens using immunoprecipitation/mass spectrometry, phage display, and protein arrays followed by animal experiments with single mAbs or mAb combinations will likely disclose their relevance for additional functional effects, the clinical phenotype, and their potential as diagnostic markers. It is tempting to speculate that the diverse non-GABA_AR reactivity against choroid plexus or blood vessels (e.g., mAb #113-201) may contribute to blood-brain barrier dysfunction and thus facilitate the entrance of further antibodies and immune cells into the CNS, similar to the role of glucose regulatory protein 78 auto-antibodies in neuromyelitis optica (Shimizu et al., 2017).

The present study confirmed the importance of isolation and detailed characterization of disease-specific human mAbs from the CSF of patients with encephalitis to foster the comprehensive understanding of humoral CNS autoimmunity. Patient-derived recombinant mAbs represent a useful research tool for multiple purposes and thereby allow the detailed investigation of disease mechanisms and the translation into animal models to recapitulate the clinical phenotype. Most importantly though, retracing the molecular mechanisms of human antibody pathogenicity will provide a refined biological view on some important clinical conditions, such as isolated psychosis or catatonia, which can occur with GABA_AR antibodies (Pettingill et al., 2015; Pollak et al., 2020). This knowledge will help to reduce the stigmatization associated with such psychiatric conditions by understanding them as autoimmune disorders that may require appropriate immunotherapy as a causative treatment in addition to antipsychotics or psychotherapy. Simultaneously, the mAbs are the starting point for the development of novel diagnostics and highly selective immunotherapies for the growing number of patients with antibody-mediated diseases.

Materials and methods

Patient sample handling

The index patients' parents have given written informed consent, and analyses were approved by the Charité University Hospital Institutional Review Board.

4 ml of CSF was collected during the acute phase of encephalitis (Nikolaus et al., 2018) and immediately processed for cell pellet cryopreservation, therefore centrifuged for 10 min at 400×g, with supernatant stored at -80°C and the pellet resuspended in 500 μl of 10% dimethyl sulfoxide, 45% fetal calf serum, 45% RPMI medium before freezing at -80°C. PPE was collected 6 d after lumbar puncture and stored at -80°C.

We used fluorescence-activated cell sorting to isolate single CD138⁺ ASCs, CD20⁺CD27⁺ MBCs, and CD20⁺CD27⁻ NMBCs from

preselected viable CD3⁻CD14⁻CD16⁻DAPI⁻ lymphocytes into 96-well PCR plates. The following antibodies were applied: anti-CD3-FITC (1:25; Miltenyi Biotec; #130-098-162), anti-CD14-FITC (1:25; Miltenyi Biotec; #130-098-063), anti-CD16-FITC (1:25; Miltenyi Biotec; #130-098-099), anti-CD20-PerCP-Vio700 (1:50; Miltenyi Biotec; #130-100-435), anti-CD27-APC-Vio770 (1:12.5; Miltenyi Biotec; #130-098-605), and anti-CD138-PE (1:50; Miltenyi; #130-098-122).

Generation of recombinant human mAbs

From single-cell cDNA Ig, genes encoding for variable domains of heavy and light chains were amplified, sequenced, and cloned into expression vectors containing the respective constant Ig domains. Sequence analysis data were confirmed by novel custom BASE software (Reincke et al., 2020). HEK cells (HEK293T) were transiently transfected with an Ig vector pair, mAb containing supernatant was harvested, and Ig concentrations were determined, all following our established protocols (Kornau et al., 2020; Kreye et al., 2016).

For reactivity screenings, supernatants were used if concentration was above 2 μg/ml. For detailed characterization of reactivity probabilities and functional assays, cell supernatants were purified using Protein G Sepharose beads, as described before (Kreye et al., 2016). For Fab fragment synthesis (inVivo BioTech), the IgG1 heavy chain vector was modified by the deletion of the part encoding for the Fc domains CH2 and CH3 in exchange for a FLAG-Tag and a His-Tag following the amino acids PKSCDKTH of the hinge region. Fab fragments were purified using immobilized metal affinity chromatography.

Primary neocortical cell cultures

Primary P0-P2 neocortical cultures were prepared from WT Wistar rats, as previously described (Turko et al., 2019). Briefly, dissected neocortex tissue was dissociated with Papain for 25 min (1.5 mg/ml; Merck) before trituration in BSA (10 mg/ml; Merck). Cells were then resuspended in Neurobasal A medium (supplemented with 1× B27, 1× Glutamax, and 100 U/ml Penicillin-Streptomycin; Thermo Fisher Scientific). Dissociated cells were grown in either 24-well or 6-well cell culture plates coated for 1 h with poly-L-lysine hydrobromide (20 μg/ml; Merck). For imaging with the luminescence plate reader, cells were plated in 500-μl droplets at 400 cells/μl (total: 2 × 10⁵ cells per well of a 24-well plate). For Western blot analysis, cells were plated in 2-ml droplets at 500 cells/μl (total: 1 × 10⁶ cells per well of a 6-well plate). Cultures were grown in humidified conditions at 37°C and 5% CO₂. Cells were cultured until 20–22 d in vitro (DIV) before antibody treatment or fixation.

Immunohistochemistry

For reactivity screening, recombinant mAbs were stained on 20-μm sagittal unfixed mouse brain sections mounted on glass slides. After thawing, tissue was rinsed with PBS, and then blocking solution (PBS supplemented with 2% BSA [Roth] and 5% Normal Goat Serum [Abcam]) was applied for 1 h at room temperature. As primary antibodies, undiluted HEK293T cell supernatants containing recombinant mAbs were incubated overnight at 4°C. After washing three times with PBS, Alexa Fluor 488-conjugated goat

anti-human IgG (1:1,000; Dianova; #109-545-003) diluted in blocking solution was added for 2 h at room temperature, before an additional three-time washing and mounting using DAPI-containing Fluoroshield.

For costainings (Fig. 1, B-E; and Fig. S2, A-D), purified recombinant human mAbs were used at 5 $\mu\text{g}/\text{ml}$, and tissue was fixed with 4% paraformaldehyde (PFA) and stained following the same protocol, but using blocking solution supplemented with 0.1% Triton X-100 (Chemsolute). For costainings, commercial antibodies rabbit anti-GABA_AR α 1 (1:250; Abcam; #ab33299), guinea pig anti-VGAT (1:500; Synaptic Systems; #131004), chicken anti-MAP2 (1:1,000; Thermo Fisher Scientific; #PA1-16751), rabbit anti-MAP2 (1:1,000; Merck; #AB5622), Alexa Fluor 568-conjugated goat anti-chicken IgG (1:500; Invitrogen; #AB_2534098), Alexa Fluor 647-conjugated goat anti-guinea pig IgG (1:1,000; Invitrogen; #A21450), and Alexa Fluor 594-conjugated goat anti-rabbit IgG (1:1,000; Dianova; #111-585-003) were used, and stainings were examined under an inverted fluorescence microscope (Olympus CKX41, Leica DMI6000) or for confocal and large-scale tiling images taken with a cooled electron multiplying charge coupled device camera (Rolera-MGi PLUS, QImaging). For β -subunit stainings (Fig. S2, F-H), unfixed murine brain sections and the commercial antibodies guinea pig anti-GABA_AR- β 1 (1:500; Synaptic Systems; #224705), guinea pig anti-GABA_AR- β 2 (1:500; Synaptic Systems; #224805), and rabbit anti-GABA_AR- β 3 (1:500; Synaptic Systems; #224403) were used.

CBA

HEK293T cells were cultured on poly-L-lysine-coated coverslips, transiently cotransfected with plasmids (kindly provided by Prof. Kneussel from the Center of Molecular Neurobiology in Hamburg, Germany) to express rat α 1 β 3 or α 1 β 3 γ 2 GABA_AR, and 48 h later used for live-cell immunostainings following our described protocol, with reduced incubation time for primary antibodies to 1 h at room temperature followed by PFA fixation.

For neuronal live-cell stainings, DIV 20–22 live WT neocortical rat neurons were stained with human mAbs for 30 min in a cell culture incubator at 37°C and 5% CO₂, then washed once before PFA fixation and secondary antibody application as above. For neuronal costainings, cultured neurons were washed and then first fixed with PFA, before application of blocking solution supplemented with 0.1% Triton X-100 for permeabilization followed by costaining procedures as described above.

GABA_AR-negative mAbs with intense tissue reactivity were screened for established neural antigens using commercial panel tests (Euroimmun AG).

Polyreactivity ELISA

Antibodies were tested for polyreactivity by ELISA as previously described (Tiller et al., 2008; Wardemann et al., 2003). High-protein binding plates were coated overnight at room temperature with six distinct antigens: 10 $\mu\text{g}/\text{ml}$ calf thymus double-stranded DNA (Sigma; #D8515), 10 $\mu\text{g}/\text{ml}$ single-stranded DNA prepared from double-stranded DNA (heated at 95°C for 30 min, immediately aliquoted, and frozen at -20°C), 10 $\mu\text{g}/\text{ml}$ LPS from *Escherichia coli* (Sigma; #L2637), 10 $\mu\text{g}/\text{ml}$ KLH (Sigma; #H8283), 10 $\mu\text{g}/\text{ml}$

Cardiolipin (Sigma; #C0563), and 5 $\mu\text{g}/\text{ml}$ human insulin (Sigma; I9278). Plates were washed, then blocked with PBS supplemented with 0.05% Tween and 1 mM EDTA before addition of mAbs diluted in DMEM (GIBCO BRL; #31331093) supplemented with 1% Nutridoma-SP (Roche; #11011375001). Plates were developed with HRP-labeled goat anti-human IgG Fc antibody (1:5,000; Dianova; #109-035-098) and 1-Step Ultra TMB ELISA Substrate Solution (Thermo Fisher Scientific; #34029) and stopped with 2 M sulfuric acid. In all assays, strongly polyreactive ED38 (Meffre et al., 2004) and weakly polyreactive eijB40 (Wardemann et al., 2003) were used as positive controls and mG053 as a negative control. The threshold for positive binding was calculated for each antigen separately as the OD450 subtracted by two SDs of eijB40.

GABA_AR subunit reactivity screening

Cell-based binding assay for GABA_AR was described previously (Ohkawa et al., 2014). In this study, we additionally cloned cDNAs of rat GABA_AR α 3 (NM_017069), α 4 (NM_080587), and β 2 (NM_012957) from rat brain total RNA by RT-PCR. COS7 cells were transfected with the indicated GABA_AR subunits. At 24 h after transfection, the cells were fixed with 2% PFA at room temperature for 20 min and blocked with PBS containing 10 mg/ml BSA for 15 min. The fixed cells were incubated with patient-derived mAbs (5 $\mu\text{g}/\text{ml}$) followed by staining with the Cy3-conjugated secondary antibody. Then, the cells were permeabilized with 0.1% Triton X-100 for 10 min, blocked with PBS containing 10 mg/ml BSA, and incubated with antibodies to individual GABA_AR subunits (underlined subunit in the illustration of Fig. 2 A), followed by staining with the Alexa Fluor 488-conjugated secondary antibody. We confirmed that any antibodies did not bind to untransfected cells that did not express the GABA_AR subunits through distinguishing untransfected cells with Hoechst dye (33342; Thermo Fisher Scientific) nucleic acid staining. Images were captured with a system (LSM5 Exciter; Carl Zeiss) equipped with a Plan Apochromat 63 \times /1.40 numerical aperture oil immersion objective lens.

The antibodies used in this screening included rabbit polyclonal antibodies to GABA_AR α 2 (1:250; Rockland Immunochemicals, Inc.; #600-401-D45), α 3 (1:250, extracellular epitope; Synaptic Systems; #224 303), α 5 (1:250; Millipore; #AB9678), β 3 (1:250; Abcam; #ab4046), and γ 2 (1:250, extracellular epitope; Synaptic Systems; #224 003); guinea pig polyclonal antibodies to GABA_A receptor β 2 (1:250; Synaptic Systems; #224 805); and mouse mAbs to GABA_A receptor α 1 (1:250; NeuroMab; #75-136), β 1 (1:250; NeuroMab; #75-137), and α 4 (1:250; NeuroMab; #73-383).

The identities of human and rat GABA_AR α 1-, α 2-, α 3-, α 4-, α 5-, β 1-, β 2-, β 3-, and γ 2-subunits in their amino acid sequence are 100%, 97%, 95%, 89%, 93%, 98%, 99%, 97%, and 99%, respectively; that of the human and mouse γ 2-subunit is 99%.

Quantification of relative binding strength on murine brain sections

Following the protocol above, serial dilutions of purified GABA_AR mAbs from 50 to 0.002 $\mu\text{g}/\text{ml}$ were used for staining of adjacent unfixed murine brain sections. Cerebellar images were recorded with identical settings and analyzed using ImageJ software, version 1.51n (developed by the National Institutes of

Health). From each image, the MFI was determined from five random regions of interest (ROIs) within the granular cell layer, secondary antibody MFI was subtracted as background, and resulting MFI values were scaled to the average MFI values from all five GABA_AR mAbs at 20 µg/ml (Wenke et al., 2019). Non-linear regression models [MFI = MFI_{max} * IgG concentration / (Half Max + IgG concentration)] under settings for one site-specific binding were generated using GraphPad Prism 8 (GraphPad Software Inc.).

Quantification of relative binding strength via flow cytometry

Following our established protocol (Ly et al., 2018), HEK293T cells were transiently cotransfected with plasmids encoding for rat or human α1-, β3-, and γ2-subunits of GABA_AR and enhanced GFP (EGFP) or EGFP only and then stained with serial dilutions of purified mAbs. From live single cells with top 30% protein expression (evaluated by EGFP signal), the MFI of the Alexa Fluor 647-conjugated goat anti-human IgG (1:400; Life Technologies) was calculated, and nonlinear regression models were determined as above.

Competition assay

400 µg of purified GABA_AR mAbs was concentrated to a volume of 100 µl using Amicon Ultra 100-kD columns (Merck) and then incubated with 40 µg CruzFluor 488 (CF488) succinimidyl ester (Santa Cruz Biotechnology) for 1 h under rotation in the dark. Unbound fluorophores were washed out using Amicon Ultra 100-kD columns. IgG concentrations were determined using an IgG ELISA. The degree of labeling (DOL) was calculated from spectrophotometer readings according to the manufacturer's instructions and by using the following formula (with ε_{IgG} = 210,000 cm⁻¹ M⁻¹, ε_{CF488} = cm⁻¹ M⁻¹, Correction Factor₂₈₀ = 0.11):

$$DOL = \frac{[Abs_{495} \times \epsilon_{IgG}]}{[\epsilon_{CF488} \times (Abs_{280} - \text{Correction Factor}_{280} \times Abs_{495})]}$$

(ATT Bioquest, 2021). The degrees of labeling obtained for the CF488-coupled mAbs were 10.9 for #113-101, 7.2 for #113-115, 10.8 for #113-175, and 17.5 for #113-198 and #113-201. CF488-coupled GABA_AR mAbs were used in serial dilutions to stain unfixed mouse sections, and binding was quantified by MFI quantification of CF488 signals to determine individual concentrations for each mAb, yielding intensities between detection threshold and signal saturation. At these concentrations (0.4 µg/ml for #113-115, 4 µg/ml for all others), CF488-coupled mAbs were costained with uncoupled mAbs in excess at 50 µg/ml, and MFIs were quantified and compared with single-staining MFIs.

Quantification of surface protein expression from cultured neurons

To quantify expression of cell surface proteins, we performed state-of-the-art biotinylation assays (Hughes et al., 2010; Ohkawa et al., 2014). In brief, DIV 20–22 rat neocortical neurons were treated with 5 µg/ml of GABA_AR or control mAb in culture medium for 16–18 h. Neurons were washed, then incubated with EZ-Link Sulfo-NHS-SS-Biotin (Thermo Fisher Scientific) for 30 min at 4°C. After quenching unbound biotin, scratched

neurons were lysed via sonification in RIPA buffer (150 mM NaCl, 1 mM EDTA, 100 mM Tris HCl, 1% Triton X-100, 1% sodium deoxycholate, and 0.1% SDS, pH 7.4, supplemented with protease inhibitor cocktail cOmplete Mini [Roche]) for 1 h at 4°C. Lysates were cleared of debris by centrifugation at 20,000× *g* for 20 min. The supernatant (whole protein fraction) was incubated with NeutrAvidin UltraLink beads (Thermo Fisher Scientific) for 3 h at 4°C, then eluted (surface proteins fraction). Samples were separated on an 8% gel using SDS-PAGE and analyzed by Western blotting. Images were recorded luminescence based on ImageQuant LAS 4000 mini and quantified using ImageQuant TL software (GE Healthcare; version 8.2).

For immunohistochemistry-based receptor quantification, we used DIV 20–22 rat neocortical neurons cultured in 24-well plates and applied identical mAb treatments as above. Neurons were stained as live cells with rabbit anti-GABA_AR α1 antibody (1:1,000; Abcam; #ab33299), then washed and fixed with 4% PFA before application of IRDye 680RD goat anti-rabbit IgG secondary antibody (1:2,000; LI-COR; #925-68071) for 2 h at room temperature and a final washing with PBS. Plates were recorded in an Odyssey CLx Imaging System (LI-COR) under high-quality resolution settings and analyzed using Image Studio Ver. 5.2 (LI-COR). For each well from a 2,000-pixel-sized circular ROI, the total pixel intensities were summed, background signals from control wells without primary antibody were subtracted, and these values were scaled to the mean from all wells under the untreated condition of this plate.

Autaptic neurons and electrophysiological recordings

Autaptic murine striatal neurons (DIV 15–18) were selected for IPSC recordings as these provide a homogeneous composition of inhibitory neurons, although with the limitation of the lack of opportunity to measure excitatory postsynaptic currents as controls. Autapses were incubated with 1 µg/ml human GABA_AR mAb or control antibody (anti-CD52; Bio-Rad; #HCA175) at 37°C for 24 h. Data collection from four independent cultures was performed as previously described (Zimmermann et al., 2015) with the following alterations. Cells were recorded in standard intra- and extracellular solutions, except for chemically induced NMDA responses, measured in extracellular solution containing 0 mM of Mg²⁺, 0.2 mM of CaCl₂, and 10 µM of glycine. All drugs were bath applied for 1 s except for GABA, which was applied for 3 s. Currents were normalized per culture to the mean of untreated recordings.

Animals

All animal experiments were performed according to the ARRIVE guidelines and were approved by the Thuringian state authorities (authorization UKJ-17-053) and UK home office guidelines. Male C57BL/6 mice were used at an age of 13–14 wk and male Wistar rats at postnatal age of 21 d (weighing 50–58 g). Animals were housed in temperature- and humidity-controlled conditions on a 12-h/12-h dark/light cycle and provided with food and water ad libitum.

Intrathecal osmotic pump infusions

An investigator not involved in the animal experiments randomized mice for assignment to the respective treatment. Animals

received mAb #113-115 either as IgG (high-dose group: 500 μg over 14 d, 1.5 $\mu\text{g}/\text{h}$, $n = 7$; low-dose group: 0.3 $\mu\text{g}/\text{h}$, $n = 6$) or as Fab fragment (equimolar [16.5 M] to 1.5 $\mu\text{g}/\text{h}$ of IgG, $n = 5$) or control mAb mGO53 as IgG (1.5 $\mu\text{g}/\text{h}$, $n = 5$).

Cerebroventricular infusion with GABA_AR mAb or control was performed using osmotic pumps (Alzet; model 1002), which were loaded the day before surgery. The following characteristics were used as previously reported (Petit-Pedrol et al., 2018; Planagumà et al., 2016): volume 100 μl , flow rate 0.25 $\mu\text{l}/\text{h}$, and duration 14 d. For surgery, mice were placed in a stereotaxic frame, and a bilateral cannula (PlasticsOne; model 3280PD-2.0/SP) was inserted into the ventricles (coordinates: 0.2 mm posterior and ± 1.00 mm lateral from bregma, depth 2.2 mm). Each arm of the cannula was connected to one osmotic pump, which was subcutaneously implanted on the back of the mice (two pumps per animal). After surgery, mice were kept single caged and were monitored daily to assess symptoms and survival and were videotaped at representative time points. Mice were sacrificed at day 15. Brain tissue was obtained and frozen in 2-methylbutane.

Quantification of receptor expression from animals treated via osmotic pumps

For Western blot analysis, cryopreserved brain hemispheres from treated mice were thawed and dounced in homogenization buffer (1X PBS, 0.32 M Sucrose, 10 mM Hepes, pH 7.4, 2 mM EDTA, and 1.6 mM PMSF, supplemented with protease inhibitor cocktail cOmplete Mini). Samples were centrifuged at 1,000 $\times g$ for 10 min. The supernatants (total cell fraction) were recentrifuged at 10,000 $\times g$ for 15 min, and the obtained supernatant was finally ultracentrifuged at 100,000 $\times g$ for 60 min. These pellets were suspended in sample buffer (membrane fraction), separated using SDS-PAGE, and analyzed by Western blotting as above.

Rat surgery: Placement of ventricular catheters, osmotic pumps, and wireless EEG transmitters

Osmotic pumps (Alzet; model 1007D) were used for cerebroventricular infusion of GABA_AR mAbs (volume 100 μl , flow rate 0.5 $\mu\text{l}/\text{h}$, and duration 7 d). The day before surgery, two osmotic pumps per animal were prepared by loading with either one mAb or IgG derived from one healthy human aged 35 yr. As the initial dose of GABA_AR #113-115 led to animal death through status epilepticus, applied amounts were reduced in subsequent animals, resulting in ranges from 40 to 120 μg human mAb (#113-115: $n = 6$, #113-175: $n = 3$, #mGO53: $n = 4$) or 6 mg of polyclonal human IgG ($n = 2$) per animal. The loaded pumps were then connected to polyethylene tubing 69-mm \times 1.14-mm diameter (PlasticsOne; C312VT) and a double osmotic pump connector intraventricular cannula (PlasticsOne; 3280PD-3.0/SPC). Pumps were left overnight in sterile saline solution at 37°C. The next day, under isoflurane anesthesia, rats were placed in a stereotaxic frame for surgery. The osmotic pumps were placed subcutaneously, and the attached cannula was inserted into the lateral ventricles (1.5 mm lateral, 0.6 mm caudal). A subcutaneous pocket was formed over the right flank with a single skin incision and blunt tissue dissection for the transmitter (OpenSource

Instruments [OSI]; A3028B-DD subcutaneous transmitters, 90-mm leads), and depth electrode (OSI; W-Electrode [SCE-W]) was placed in the left hippocampus (CA3, 3.5 mm lateral, 3.6 mm caudal, depth 2.3 mm) with reference electrode implanted in the contralateral skull (3.5 mm lateral, 3.6 mm caudal). The cannula and skull electrodes were secured with dental cement as previously described (Wright et al., 2015). Placement of catheters and electrodes was assessed postmortem during preparation of brain slices for electrophysiology and immunostaining.

Collection and analysis of EEG data

A custom-built Faraday cage with aerial was used to collect and record EEG data. Transmitter signals were continuously recorded in animals while freely moving using Neuroarchiver software (OSI) and analyzed as previously described (Wright et al., 2015; Wykes et al., 2012). In brief, the EEG coastline length was measured as the cumulative absolute difference in voltage between consecutive data points (Korn et al., 1987). For automated ictal event detection, video-EEG matching was used to identify ictal EEG events. The Event Classifier (OSI) was then used to classify 1-s segments of EEG according to several metrics, enabling similar events to cluster together when plotted according to metrics. This generated a library of ictal events that allowed fast identification of abnormal EEG events by automated comparison to the library (http://www.opensourceinstruments.com/Electronics/A3018/Seizure_Detection.html). Powerband analysis was performed using a custom-designed macro.

Behavioral tests

The PSBB was used to monitor long-term behavioral changes during and after the GABA_AR antibody infusion (two tests were performed each week for the 3-wk recording period in $n = 3$ animals). The behavioral task consists of two simple and non-stressful tasks (i.e., touch and pickup tasks). If the product of these scores is >10 , the animals are highly likely to have developed hyperexcitability and aggression; these measures strongly correlate with the development of spontaneous recurrent seizures (Modebadze et al., 2016).

Local field potential recordings

At the end of the recording period, 450- μm brain slices were prepared from the GABA_AR and control mAb-infused rats and used for hippocampal local field potential recordings as previously described (Johnson et al., 2017; Modebadze et al., 2016). Local field potential recordings were assessed using Spike2 software (CED) for spontaneous epileptiform activity. Spike2 was used to calculate the root mean square amplitude of each recording. Epileptiform activity was classified as an event when it displayed amplitudes greater than fourfold the root mean square amplitude, providing the event count, while the time difference between these events provided the interevent interval. Measurements are expressed as median, interquartile range, and min-max values.

Statistical analysis

All statistical analyses were conducted using GraphPad Prism 8 (GraphPad Software Inc.). For sequence analysis, numbers of

somatic hypermutations were compared using an ordinary one-way ANOVA test followed by post hoc Tukey's multiple comparisons tests. Amplitudes from autaptic neuron recordings were tested using Kruskal-Wallis, Dunn's post hoc tests. Protein expression quantifications from Western blotting and immunohistochemistry data were analyzed with ordinary one-way ANOVA tests followed by post hoc Tukey's multiple comparisons tests. Kaplan-Meier survival analysis was analyzed by log-rank (Mantel-Cox) test followed by ANOVA with post hoc Tukey's multiple comparisons tests. Coastline length measurements, ictal event counts, and power averages from in vivo EEG recordings and interevent intervals of spontaneous ictal activity from postmortem acute brain slice recordings were analyzed using Mann-Whitney tests.

Online supplemental material

Fig. S1 supplements **Fig. 1** and shows the identification of GABA_AR mAbs, their Ig sequence features, and polyreactivity data. **Fig. S2** supplements **Fig. 1** and shows further immunofluorescence stainings of patient-derived and commercial GABA_AR mAbs on murine brain tissue. **Fig. S3** supplements **Fig. 2** and shows specificity and binding strength data of GABA_AR mAbs. **Fig. S4** supplements **Fig. 3** and provides data from control experiments for the quantification of protein expression from cultured neurons treated with GABA_AR mAbs. **Fig. S5** supplements **Fig. 4** and **Fig. 5** and provides the characterization of GABA_AR Fab #113-115 and animal data from prolonged EEG recordings and behavioral testing after cerebroventricular infusion of GABA_AR mAbs. Table S1 presents sequence and reactivity data from GABA_AR encephalitis CSF antibody repertoire. It lists Ig sequence features and reactivity characteristics for mAbs with corresponding identifier (mAb ID) isolated from CSF cells of different phenotypes, including ASCs, MBCs, and NMBCs. Table S2 shows regression models for GABA_AR mAb binding to unfixed murine brain. Table S3 characterizes disease symptomatology in GABA_AR encephalitis mouse model. **Video 1** shows catatonia and epileptic seizures in mice after intrathecal infusion of GABA_AR mAbs. **Video 2** is a recording of a Racine stage 5 seizure in a rat after intrathecal infusion of GABA_AR.

Data availability

Raw data were generated at the German Center for Neurodegenerative Diseases (DZNE) Berlin, Charité University Medicine Berlin, Aston University Birmingham, University Hospital Jena, and National Institute for Physiological Sciences Okazaki. All relevant data supporting the key findings of this study are available within the article and its supplementary information files. The sequencing information for all mAbs from this manuscript, including raw data files and data derived from custom BASE software analysis, have been deposited to Code Ocean (<https://doi.org/10.24433/CO.5442144.v1>). The custom software BASE used for Ig sequence analysis is available at <https://github.com/automatedSequencing/BASE>.

Acknowledgments

We thank Doreen Brandl, Matthias Sillmann, and Stefanie Bandura (DZNE, Berlin, Germany) for excellent technical assistance

and Rob Wykes, Jonathan Cornford, and Andrea Lieb (University College London, UK) for use of the electroencephalography powerband analysis program.

This work was supported by the German Research Foundation (SFB1315 to A.M. Kaindl; FOR3004 to A.M. Kaindl, C. Geis, and H. Prüss; GE2519/8-1 and GE2519/9-1 to C. Geis; EXC2049 to D. Schmitz; PR 1274/2-1, PR 1274/3-1, and PR 1274/5-1 to H. Prüss), by the Helmholtz Association (HIL-A03 to H. Prüss), by the German Federal Ministry of Education and Research (Connect-Generate 01GM1908D to H. Prüss and 01GM1908B to C. Geis), by a BIH-Charité Junior Clinician Scientist Fellowship funded by Charité – Universitätsmedizin Berlin and the Berlin Institute of Health (to J. Kreye and S. Momsen Reincke), by the Academy of Medical Sciences (SBF004\1053 to D.R. Dhangar), by an Epilepsy Research UK Fellowship and Wellcome Trust Clinical Research Career Development Fellowship (to S.K. Wright), by the Schilling foundation (to C. Geis), the Interdisciplinary Center of Clinical Research of the Medical Faculty Jena (to J. Wickel), Japan Society for the Promotion of Science/Ministry of Education, Culture, Sports, Science, and Technology KAKENHI (19H03331, 19K22439 to Y. Fukata; 20H00459, 19K22548 to M. Fukata), DAIKO Foundation (to Y. Fukata), and the Hori Sciences and Arts Foundation (to M. Fukata). This research was funded in whole or in part by Wellcome Trust. For the purpose of Open Access, the author has applied a CC-BY public copyright license to any Author Accepted Manuscript (AAM) version arising from this submission.

Author contributions: J. Kreye, S.K. Wright, and H. Prüss designed the study. J. Kreye, S.K. Wright, A. van Casteren, L. Stöffler, M.-L. Machule, M. Nikolaus, S. van Hoof, E. Sanchez-Sendin, M.A. Homeyer, C. Cordero Gómez, M.A. Wilson, M.A. Upadhyaya, D.R. Dhangar, S. Greenhill, P. Turko, J. Wickel, Y. Fukata, and M. Fukata acquired data. J. Kreye, S.K. Wright, A. van Casteren, L. Stöffler, M.-L. Machule, S. Momsen Reincke, M. Nikolaus, H.-C. Kornau, D. Schmitz, A.M. Kaindl, P. Boehm-Sturm., S. Mueller, M.A. Wilson, S. Greenhill, G. Woodhall, P. Turko, I. Vida, C.C. Garner, J. Wickel, C. Geis, Y. Fukata, M. Fukata, and H. Prüss analyzed and interpreted data. J. Kreye, S.K. Wright, and H. Prüss drafted the manuscript. All authors have critically revised and approved the submitted version.

Disclosures: No disclosures were reported.

Submitted: 18 January 2021

Revised: 30 June 2021

Accepted: 17 August 2021

References

- ATT Bioquest. 2021. Degree of Labeling (DOL) Calculator. <https://www.aatbio.com/tools/degree-of-labeling-calculator> (accessed June 28, 2021)
- Bracher, A., C. Alcalá, J. Ferrer, N. Melzer, R. Hohlfeld, B. Casanova, E. Beltrán, and K. Dornmair. 2020. An expanded parenchymal CD8⁺ T cell clone in GABA_A receptor encephalitis. *Ann. Clin. Transl. Neurol.* 7: 239–244. <https://doi.org/10.1002/acn3.50974>
- Brändle, S.M., M. Cerina, S. Weber, K. Held, A.F. Menke, C. Alcalá, D. Gebert, A.M. Herrmann, H. Pellkofer, L.A. Gerdes, et al. 2021. Cross-reactivity of a pathogenic autoantibody to a tumor antigen in GABA_A receptor encephalitis. *Proc. Natl. Acad. Sci. USA.* 118:e1916337118. <https://doi.org/10.1073/pnas.1916337118>

- Crisp, S.J., C.L. Dixon, L. Jacobson, E. Chabrol, S.R. Irani, M.I. Leite, G. Leschziner, S.J. Slaght, A. Vincent, and D.M. Kullmann. 2019. Glycine receptor autoantibodies disrupt inhibitory neurotransmission. *Brain*. 142:3398–3410. <https://doi.org/10.1093/brain/awz297>
- Ebert, V., P. Scholze, K. Fuchs, and W. Sieghart. 1999. Identification of subunits mediating clustering of GABA(A) receptors by rapsyn. *Neurochem. Int.* 34:453–463. [https://doi.org/10.1016/S0197-0186\(99\)00039-X](https://doi.org/10.1016/S0197-0186(99)00039-X)
- Farrant, M., and Z. Nusser. 2005. Variations on an inhibitory theme: phasic and tonic activation of GABA(A) receptors. *Nat. Rev. Neurosci.* 6:215–229. <https://doi.org/10.1038/nrn1625>
- Hernandez, C.C., W. XiangWei, N. Hu, D. Shen, W. Shen, A.H. Lagrange, Y. Zhang, L. Dai, C. Ding, Z. Sun, et al. 2019. Altered inhibitory synapses in de novo GABRA5 and GABRA1 mutations associated with early onset epileptic encephalopathies. *Brain*. 142:1938–1954. <https://doi.org/10.1093/brain/awz123>
- Höftberger, R., L. Sabater, A. Ortega, J. Dalmau, and F. Graus. 2013. Patient with homer-3 antibodies and cerebellitis. *JAMA Neurol.* 70:506–509. <https://doi.org/10.1001/jamaneurol.2013.1955>
- Hughes, E.G., X. Peng, A.J. Gleichman, M. Lai, L. Zhou, R. Tsou, T.D. Parsons, D.R. Lynch, J. Dalmau, and R.J. Balice-Gordon. 2010. Cellular and synaptic mechanisms of anti-NMDA receptor encephalitis. *J. Neurosci.* 30:5866–5875. <https://doi.org/10.1523/JNEUROSCI.0167-10.2010>
- Jézéquel, J., E.M. Johansson, J.P. Dupuis, V. Rogemond, H. Gréa, B. Keller-mayer, N. Hamdani, E. Le Guen, C. Rabu, M. Lepleux, et al. 2017. Dynamic disorganization of synaptic NMDA receptors triggered by autoantibodies from psychotic patients. *Nat. Commun.* 8:1791. <https://doi.org/10.1038/s41467-017-01700-3>
- Johnson, N.W., M. Özkan, A.P. Burgess, E.J. Prokic, K.A. Wafford, M.J. O'Neill, S.D. Greenhill, I.M. Stanford, and G.L. Woodhall. 2017. Phase-amplitude coupled persistent theta and gamma oscillations in rat primary motor cortex in vitro. *Neuropharmacology*. 119:141–156. <https://doi.org/10.1016/j.neuropharm.2017.04.009>
- Jones, R.S., and U. Heinemann. 1988. Synaptic and intrinsic responses of medial entorhinal cortical cells in normal and magnesium-free medium in vitro. *J. Neurophysiol.* 59:1476–1496. <https://doi.org/10.1152/jn.1988.59.5.1476>
- Korn, S.J., J.L. Giacchino, N.L. Chamberlin, and R. Dingledine. 1987. Epileptiform burst activity induced by potassium in the hippocampus and its regulation by GABA-mediated inhibition. *J. Neurophysiol.* 57:325–340. <https://doi.org/10.1152/jn.1987.57.1.325>
- Kornau, H.C., J. Kreye, A. Stumpf, Y. Fukata, D. Parthier, R.P. Sammons, B. Imbrosci, S. Kurpjuweit, A.B. Kowski, M. Fukata, et al. 2020. Human Cerebrospinal Fluid Monoclonal LGII Autoantibodies Increase Neuronal Excitability. *Ann. Neurol.* 87:405–418. <https://doi.org/10.1002/ana.25666>
- Kreye, J., N.K. Wenke, M. Chayka, J. Leubner, R. Murugan, N. Maier, B. Jurek, L.T. Ly, D. Brandl, B.R. Rost, et al. 2016. Human cerebrospinal fluid monoclonal N-methyl-D-aspartate receptor autoantibodies are sufficient for encephalitis pathogenesis. *Brain*. 139:2641–2652. <https://doi.org/10.1093/brain/aww208>
- Kreye, J., S.M. Reincke, H.C. Kornau, E. Sánchez-Sendin, V.M. Corman, H. Liu, M. Yuan, N.C. Wu, X. Zhu, C.D. Lee, et al. 2020. A therapeutic non-self-reactive SARS-CoV-2 antibody protects from lung pathology in a COVID-19 hamster model. *Cell*. 183:1058–1069.e19. <https://doi.org/10.1016/j.cell.2020.09.049>
- Lachance-Touchette, P., C. Martin, C. Poulin, M. Gravel, L. Carmant, and P. Cossette. 2010. Screening of GABRB3 in French-Canadian families with idiopathic generalized epilepsy. *Epilepsia*. 51:1894–1897. <https://doi.org/10.1111/j.1528-1167.2010.02642.x>
- Ladépêche, L., J. Planagumà, S. Thakur, I. Suárez, M. Hara, J.S. Borbely, A. Sandoval, L. Laparra-Cuervo, J. Dalmau, and M. Lakadamyali. 2018. NMDA Receptor Autoantibodies in Autoimmune Encephalitis Cause a Subunit-Specific Nanoscale Redistribution of NMDA Receptors. *Cell Rep.* 23:3759–3768. <https://doi.org/10.1016/j.celrep.2018.05.096>
- Lüttjohann, A., P.F. Fabene, and G. van Luijtelaar. 2009. A revised Racine's scale for PTZ-induced seizures in rats. *Physiol. Behav.* 98:579–586. <https://doi.org/10.1016/j.physbeh.2009.09.005>
- Ly, L.T., J. Kreye, B. Jurek, J. Leubner, F. Scheibe, J. Lemcke, N.K. Wenke, S.M. Reincke, and H. Prüss. 2018. Affinities of human NMDA receptor autoantibodies: implications for disease mechanisms and clinical diagnostics. *J. Neurol.* 265:2625–2632. <https://doi.org/10.1007/s00415-018-9042-1>
- Maljevic, S., K. Krampfl, J. Cobilanschi, N. Tilgen, S. Beyer, Y.G. Weber, F. Schlesinger, D. Ursu, W. Melzer, P. Cossette, et al. 2006. A mutation in the GABA(A) receptor alpha(1)-subunit is associated with absence epilepsy. *Ann. Neurol.* 59:983–987. <https://doi.org/10.1002/ana.20874>
- Malviya, M., S. Barman, K.S. Golombeck, J. Planagumà, F. Mannara, N. Strutz-Seebohm, C. Wrzos, F. Demir, C. Baksmeier, J. Steckel, et al. 2017. NMDAR encephalitis: passive transfer from man to mouse by a recombinant antibody. *Ann. Clin. Transl. Neurol.* 4:768–783. <https://doi.org/10.1002/acn3.444>
- Meffre, E., A. Schaefer, H. Wardemann, P. Wilson, E. Davis, and M.C. Nus-senzweig. 2004. Surrogate light chain expressing human peripheral B cells produce self-reactive antibodies. *J. Exp. Med.* 199:145–150. <https://doi.org/10.1084/jem.20031550>
- Miller, P.S., and A.R. Aricescu. 2014. Crystal structure of a human GABAA receptor. *Nature*. 512:270–275. <https://doi.org/10.1038/nature13293>
- Modebadze, T., N.H. Morgan, I.A. Pérès, R.D. Hadid, N. Amada, C. Hill, C. Williams, I.M. Stanford, C.M. Morris, R.S. Jones, et al. 2016. A Low Mortality, High Morbidity Reduced Intensity Status Epilepticus (RISE) Model of Epilepsy and Epileptogenesis in the Rat. *PLoS One*. 11:e0147265. <https://doi.org/10.1371/journal.pone.0147265>
- Nikolaus, M., E. Knierim, C. Meisel, J. Kreye, H. Prüss, D. Schnabel, and T. Kallinich. 2018. Severe GABA_A receptor encephalitis without seizures: A paediatric case successfully treated with early immunomodulation. *Eur. J. Paediatr. Neurol.* 22:558–562. <https://doi.org/10.1016/j.ejpn.2018.01.002>
- Ohkawa, T., S. Satake, N. Yokoi, Y. Miyazaki, T. Ohshita, G. Sobue, H. Takashima, O. Watanabe, Y. Fukata, and M. Fukata. 2014. Identification and characterization of GABA(A) receptor autoantibodies in autoimmune encephalitis. *J. Neurosci.* 34:8151–8163. <https://doi.org/10.1523/JNEUROSCI.4415-13.2014>
- Olsen, R.W., and W. Sieghart. 2008. International Union of Pharmacology. LXX. Subtypes of gamma-aminobutyric acid(A) receptors: classification on the basis of subunit composition, pharmacology, and function. Update. *Pharmacol. Rev.* 60:243–260. <https://doi.org/10.1124/pr.108.00505>
- Petit-Pedrol, M., T. Armangue, X. Peng, L. Bataller, T. Cellucci, R. Davis, L. McCracken, E. Martínez-Hernandez, W.P. Mason, M.C. Kruer, et al. 2014. Encephalitis with refractory seizures, status epilepticus, and antibodies to the GABAA receptor: a case series, characterisation of the antigen, and analysis of the effects of antibodies. *Lancet Neurol.* 13:276–286. [https://doi.org/10.1016/S1474-4422\(13\)70299-0](https://doi.org/10.1016/S1474-4422(13)70299-0)
- Petit-Pedrol, M., J. Sell, J. Planagumà, F. Mannara, M. Radosevic, H. Haselmann, M. Ceanga, L. Sabater, M. Spatola, D. Soto, et al. 2018. LGII antibodies alter Kv1.1 and AMPA receptors changing synaptic excitability, plasticity and memory. *Brain*. 141:3144–3159. <https://doi.org/10.1093/brain/awy253>
- Pettingill, P., H.B. Kramer, J.A. Coebergh, R. Pettingill, S. Maxwell, A. Nibber, A. Malaspina, A. Jacob, S.R. Irani, C. Buckley, et al. 2015. Antibodies to GABA_A receptor α 1 and γ 2 subunits: clinical and serologic characterization. *Neurology*. 84:1233–1241. <https://doi.org/10.1212/WNL.0000000000001326>
- Planagumà, J., F. Leypoldt, F. Mannara, J. Gutiérrez-Cuesta, E. Martín-García, E. Aguilar, M.J. Titulaer, M. Petit-Pedrol, A. Jain, R. Balice-Gordon, et al. 2015. Human N-methyl D-aspartate receptor antibodies alter memory and behaviour in mice. *Brain*. 138:94–109. <https://doi.org/10.1093/brain/awu310>
- Planagumà, J., H. Haselmann, F. Mannara, M. Petit-Pedrol, B. Grünewald, E. Aguilar, L. Röpke, E. Martín-García, M.J. Titulaer, P. Jercoc, et al. 2016. Ephrin-B2 prevents N-methyl-D-aspartate receptor antibody effects on memory and neuroplasticity. *Ann. Neurol.* 80:388–400. <https://doi.org/10.1002/ana.24721>
- Pollak, T.A., B.R. Lennox, S. Müller, M.E. Benros, H. Prüss, L. Tebartz van Elst, H. Klein, J. Steiner, T. Frodl, B. Bogerts, et al. 2020. Autoimmune psychosis: an international consensus on an approach to the diagnosis and management of psychosis of suspected autoimmune origin. *Lancet Psychiatry*. 7:93–108. [https://doi.org/10.1016/S2215-0366\(19\)30290-1](https://doi.org/10.1016/S2215-0366(19)30290-1)
- Puttachary, S., S. Sharma, K. Tse, E. Beamer, A. Sexton, J. Crutison, and T. Thippeswamy. 2015. Immediate Epileptogenesis after Kainate-Induced Status Epilepticus in C57BL/6j Mice: Evidence from Long Term Continuous Video-EEG Telemetry. *PLoS One*. 10:e0131705. <https://doi.org/10.1371/journal.pone.0131705>
- Ramberger, M., A. Berretta, J.M.M. Tan, B. Sun, S. Michael, T. Yeo, J. Theorell, R. Bashford-Rogers, S. Paneva, V. O'Dowd, et al. 2020. Distinctive binding properties of human monoclonal LGII autoantibodies determine pathogenic mechanisms. *Brain*. 143:1731–1745. <https://doi.org/10.1093/brain/awaa104>
- Rasmussen, S.G., B.T. DeVree, Y. Zou, A.C. Kruse, K.Y. Chung, T.S. Kobilka, F.S. Thian, P.S. Chae, E. Pardon, D. Calinski, et al. 2011. Crystal structure of the β 2 adrenergic receptor-Gs protein complex. *Nature*. 477:549–555. <https://doi.org/10.1038/nature10361>

- Reincke, S.M., H. Prüss, and J. Kreye. 2020. Brain antibody sequence evaluation (BASE): an easy-to-use software for complete data analysis in single cell immunoglobulin cloning. *BMC Bioinformatics*. 21:446. <https://doi.org/10.1186/s12859-020-03741-w>
- Sharma, R., F.H. Al-Saleem, J. Panzer, J. Lee, R.D. Puligedda, L.F. Felicori, C.D. Kattala, A.J. Rattelle, G. Ippolito, R.H. Cox, et al. 2018. Monoclonal antibodies from a patient with anti-NMDA receptor encephalitis. *Ann. Clin. Transl. Neurol.* 5:935–951. <https://doi.org/10.1002/acn3.592>
- Shimizu, F., K.L. Schaller, G.P. Owens, A.C. Cotleur, D. Kellner, Y. Takeshita, B. Obermeier, T.J. Kryzer, Y. Sano, T. Kanda, et al. 2017. Glucose-regulated protein 78 autoantibody associates with blood-brain barrier disruption in neuromyelitis optica. *Sci. Transl. Med.* 9:eaai9111. <https://doi.org/10.1126/scitranslmed.aai9111>
- Spatola, M., M. Petit-Pedrol, M.M. Simabukuro, T. Armangue, F.J. Castro, M.I. Barcelo Artigues, M.R. Julià Benique, L. Benson, M. Gorman, A. Felipe, et al. 2017. Investigations in GABA_A receptor antibody-associated encephalitis. *Neurology*. 88:1012–1020. <https://doi.org/10.1212/WNL.0000000000003713>
- Symmonds, M., C.H. Moran, M.I. Leite, C. Buckley, S.R. Irani, K.E. Stephan, K.J. Friston, and R.J. Moran. 2018. Ion channels in EEG: isolating channel dysfunction in NMDA receptor antibody encephalitis. *Brain*. 141:1691–1702. <https://doi.org/10.1093/brain/awy107>
- Tiller, T., E. Meffre, S. Yurasov, M. Tsuiji, M.C. Nussenzweig, and H. Wardemann. 2008. Efficient generation of monoclonal antibodies from single human B cells by single cell RT-PCR and expression vector cloning. *J. Immunol. Methods*. 329:112–124. <https://doi.org/10.1016/j.jim.2007.09.017>
- Turko, P., K. Groberman, T. Kaiser, Y. Yanagawa, and I. Vida. 2019. Primary Cell Culture of Purified GABAergic or Glutamatergic Neurons Established through Fluorescence-activated Cell Sorting. *J. Vis. Exp.* (148). <https://doi.org/10.3791/58974>
- Wallace, R.H., C. Marini, S. Petrou, L.A. Harkin, D.N. Bowser, R.G. Panchal, D.A. Williams, G.R. Sutherland, J.C. Mulley, I.E. Scheffer, and S.F. Berkovic. 2001. Mutant GABA(A) receptor gamma2-subunit in childhood absence epilepsy and febrile seizures. *Nat. Genet.* 28:49–52. <https://doi.org/10.1038/ng0501-49>
- Wardemann, H., S. Yurasov, A. Schaefer, J.W. Young, E. Meffre, and M.C. Nussenzweig. 2003. Predominant autoantibody production by early human B cell precursors. *Science*. 301:1374–1377. <https://doi.org/10.1126/science.1086907>
- Wenke, N.K., J. Kreye, E. Andrzejak, A. van Casteren, J. Leubner, M.S. Murgueitio, S.M. Reincke, C. Secker, L. Schmidl, C. Geis, et al. 2019. N-methyl-D-aspartate receptor dysfunction by unmutated human antibodies against the NR1 subunit. *Ann. Neurol.* 85:771–776. <https://doi.org/10.1002/ana.25460>
- Wright, S., K. Hashemi, L. Stasiak, J. Bartram, B. Lang, A. Vincent, and A.L. Upton. 2015. Epileptogenic effects of NMDAR antibodies in a passive transfer mouse model. *Brain*. 138:3159–3167. <https://doi.org/10.1093/brain/awv257>
- Wykes, R.C., J.H. Heeroma, L. Mantoan, K. Zheng, D.C. MacDonald, K. Deisseroth, K.S. Hashemi, M.C. Walker, S. Schorge, and D.M. Kullmann. 2012. Optogenetic and potassium channel gene therapy in a rodent model of focal neocortical epilepsy. *Sci. Transl. Med.* 4:161ra152. <https://doi.org/10.1126/scitranslmed.3004190>
- Zimmermann, J., M.A. Herman, and C. Rosenmund. 2015. Co-release of glutamate and GABA from single vesicles in GABAergic neurons exogenously expressing VGLUT3. *Front. Synaptic Neurosci.* 7:16. <https://doi.org/10.3389/fnsyn.2015.00016>

Supplemental material

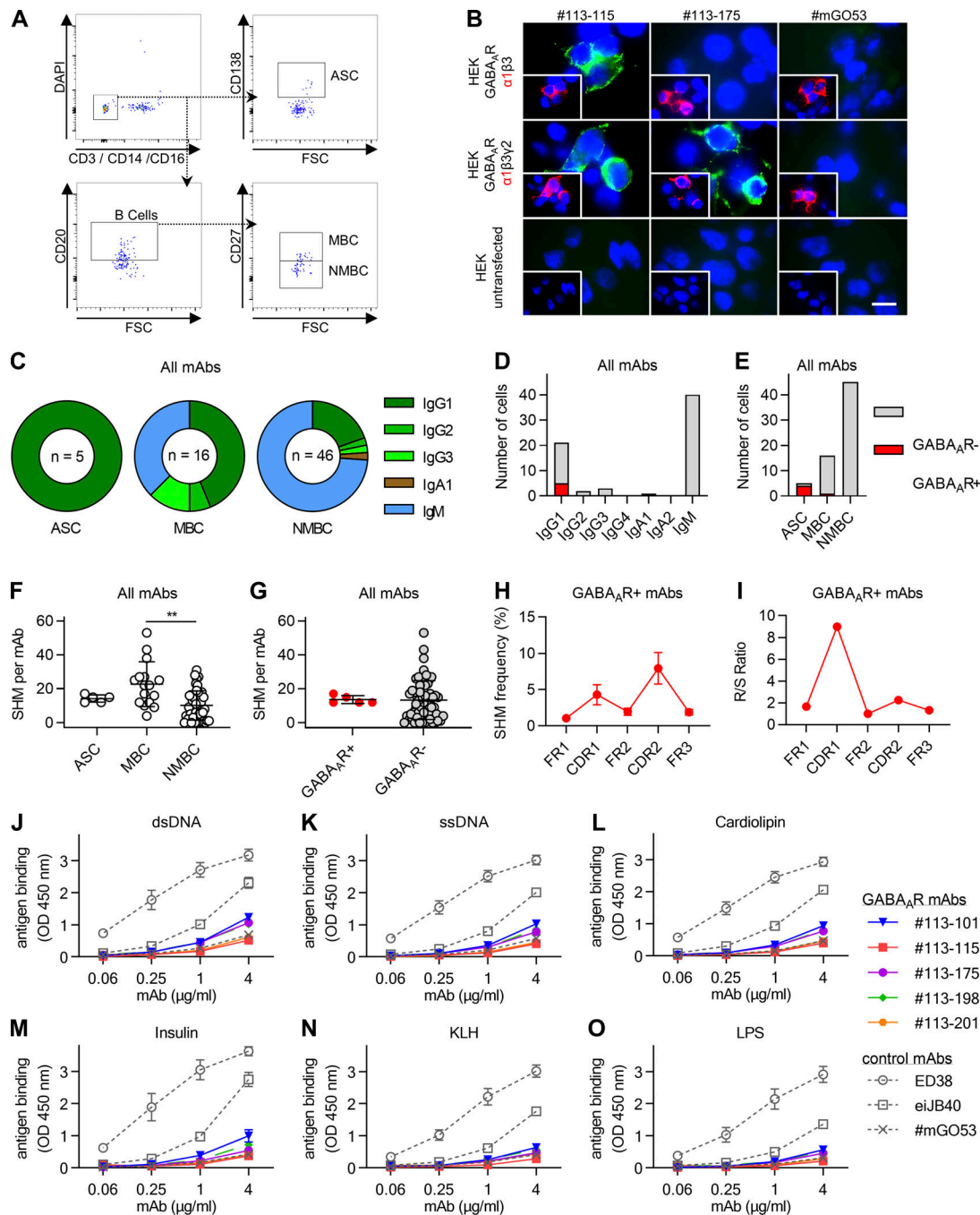


Figure S1. Characterization of reactivity and Ig sequence features from mAbs of GABA_AR encephalitis CSF repertoire. (A) Gating strategy in fluorescence-activated cell sorting is shown for isolation of CSF single cells for recombinant mAb cloning. CD3⁻CD14⁻CD16⁻DAPI⁻ lymphocytes (top left) were gated for CD138⁺ antibody-secreting cells (top right) or CD20⁺ B cells (bottom left), further differentiated into CD27⁺ MBCs and CD27⁻ NMBCs (bottom right). (B) Immunofluorescence stainings of recombinant human mAbs (green, as indicated in column caption) to HEK cells overexpressing the α1β3- or α1β3γ2-subunits of GABA_AR or untransfected controls (as indicated in row caption). Costaining with commercial α1-specific antibody is shown in red and nuclei staining with DAPI in blue. Representative scale bar indicates 20 μm. (C) Ig subclass distributions per mAb source cell type from GABA_AR encephalitis CSF repertoire. (D and E) Absolute frequencies of GABA_AR-reactive (GABA_AR⁺) and GABA_AR-negative (GABA_AR⁻) mAbs per Ig subclass (D) and mAb source cell type (E). (F) Comparison of SHM counts in the variable domain V genes between mAbs of different source cell types, analyzed using ordinary one-way ANOVA followed by post hoc Tukey's multiple comparison (**, $P \leq 0.01$; or not shown when $P > 0.05$). Each dot indicates one mAb, $n = 5-46$ mAbs per group. Bars indicate mean \pm SD. (G) Comparison of SHM counts in the variable domain V genes between GABA_AR⁺ and GABA_AR⁻ mAbs. Each dot indicates one mAb, $n = 5-62$ mAbs per group. Bars indicate mean \pm SD. (H) Relative frequencies of SHM per nucleotide within CDRs and FRs of GABA_AR⁺ mAb genes, shown as mean \pm SEM; $n = 5$. (I) Mean ratios of replacement to silence (R/S) mutations within CDRs and FRs for all SHMs of all GABA_AR⁺ mAb genes combined. (J-O) Concentration-dependent binding of GABA_AR⁺ mAbs to indicated polyreactivity-defining antigens in an ELISA-based assay in comparison to controls of strongly polyreactive ED38, weakly polyreactive eiJB40, and nonpolyreactive #mGO53. Bars indicate mean \pm SEM from duplicate measurements of $n = 2$ independent experiments. All stainings were replicated at least twice on tissue or neurons from two different animals. dsDNA, double-stranded DNA; FSC, forward scatter; ssDNA, single-stranded DNA.

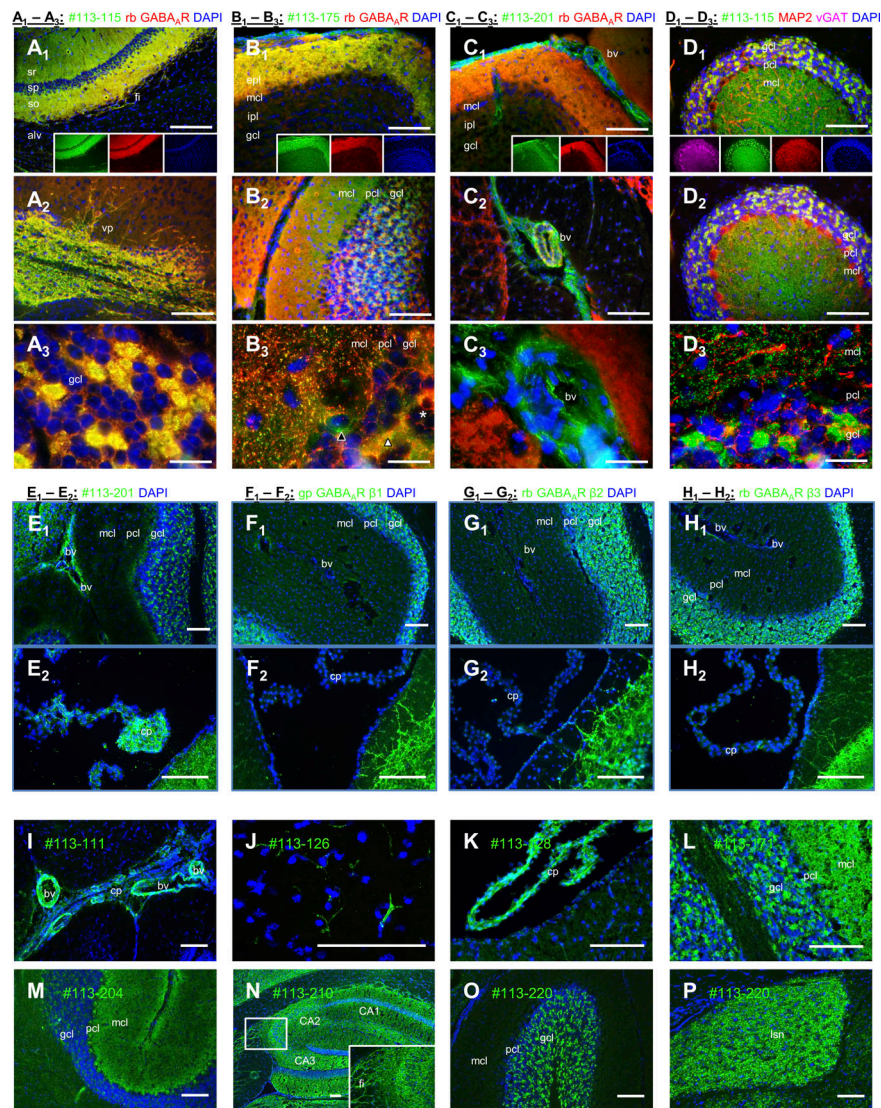


Figure S2. **Brain tissue reactivity patterns of human GABA_AR and GABA_AR-negative mAbs.** (A–D) Immunofluorescence stainings of selected human GABA_AR mAbs (green; DAPI nuclei in blue) on fixed murine brain tissue in costainings with commercial antibodies (red/pink) as indicated in the column caption above. (A₁) #113-115 intensively stained hippocampal neuropil throughout CA1 and CA2, most pronounced in stratum oriens (so) with hippocampal fimbria (fi) and stratum radiatum (sr), revealing complete overlap with commercial α 1-specific antibody-binding pattern (red; merge in yellow). (A₂) Both antibodies showed distinct staining of the ventral pallidum. (A₃) Higher magnifications in confocal acquisition revealed a somatic staining pattern with complete overlap in the granule cell layer (gcl) of the cerebellum. (B₁) α 1 γ 2-dependent #113-175 stained the olfactory bulb, overlapping with commercial α 1-specific antibody, most pronounced in the external plexiform layer (epl) and the molecular cell layer (mcl), whereas weaker in the internal plexiform layer (ipl) and the gcl. (B₂ and B₃) In the cerebellum, the mcl and gcl patterns uncovered different GABA_AR-expressing cell populations, some predominantly labeled by #113-175 (green, black arrowhead), some by commercial antibody (red, white asterisk), and others equally double positive (yellow, white arrowhead). (C₁) #113-201 and commercial α 1-specific antibody targeted the epl of the olfactory bulb. (C₂ and C₃) However, #113-201 additionally showed intense binding around blood vessels (bv) and choroid plexus (cp), still detectable at dilutions below the GABA_AR pattern detection (not shown). (D₁) In cerebellar stainings, human mAb GABA_AR-binding pattern (shown for #113-115) clearly distinguished from MAP2-positive dendrites, most pronounced in the mcl (D₂) and from vGAT-highlighted somata of the pcl. (D₃) In magnified confocal images, human mAb visualized GABA_AR clusters throughout the mcl and on a subpopulation of cells within the gcl, shown with a reticular MAP2 costaining. (E–H) Immunofluorescence stainings on unfixed murine brain tissue of human GABA_AR mAb #113-201 or commercial antibodies specific for indicated GABA_AR β -subunits (green; DAPI nuclei in blue). mAb #113-201 bound to the gcl of the cerebellum with expected GABA_AR expression, but additionally also around blood vessels (bv) between the mcl of two neighboring gyri (E₁) and to the choroid plexus (cp) in the ventricles (E₂). Binding of β -subunit-specific antibodies was not detected (F₁, G₁, and H₁) around blood vessels or in choroid plexus (F₂, G₂, and H₂), therefore indicating GABA_AR-independent binding of #113-201 in these locations, as β -subunits are essential for functional GABA_ARs. (I–P) Immunofluorescence stainings of human GABA_AR-negative mAbs (green; nuclei in blue) from GABA_AR encephalitis patient’s CSF repertoire. (I) Germline mAb #113-111 highlighted large bv and cp tissue. (J) #113-126 stained fine vessels, specifically in frontal cortex. (K) #113-128 targeted cp. (L) #113-171, the only GABA_AR-negative mAb derived from an ASC, showed a similar staining pattern as GABA_AR mAbs, including intensive binding to the gcl and mcl molecular but not pcl of the cerebellum. (M) #113-204 was reactive to the mcl and pcl of the cerebellum. (N) #113-210 stained intensively hippocampal neuropil, pronounced in the CA2 and CA3 region, fimbria of the hippocampus (fi). (O and P) #113-220 targeted selectively granule cells in the cerebellum and revealed a punctuated pattern in the lateral septal nuclei. Scale bars indicate 100 μ m, 20 μ m in the third row (A₃–D₃). alv, alveus; gp, guinea pig; pcl, Purkinje cell layer; rb, rabbit; sp, stratum pyramidale; vp, ventral pallidum.

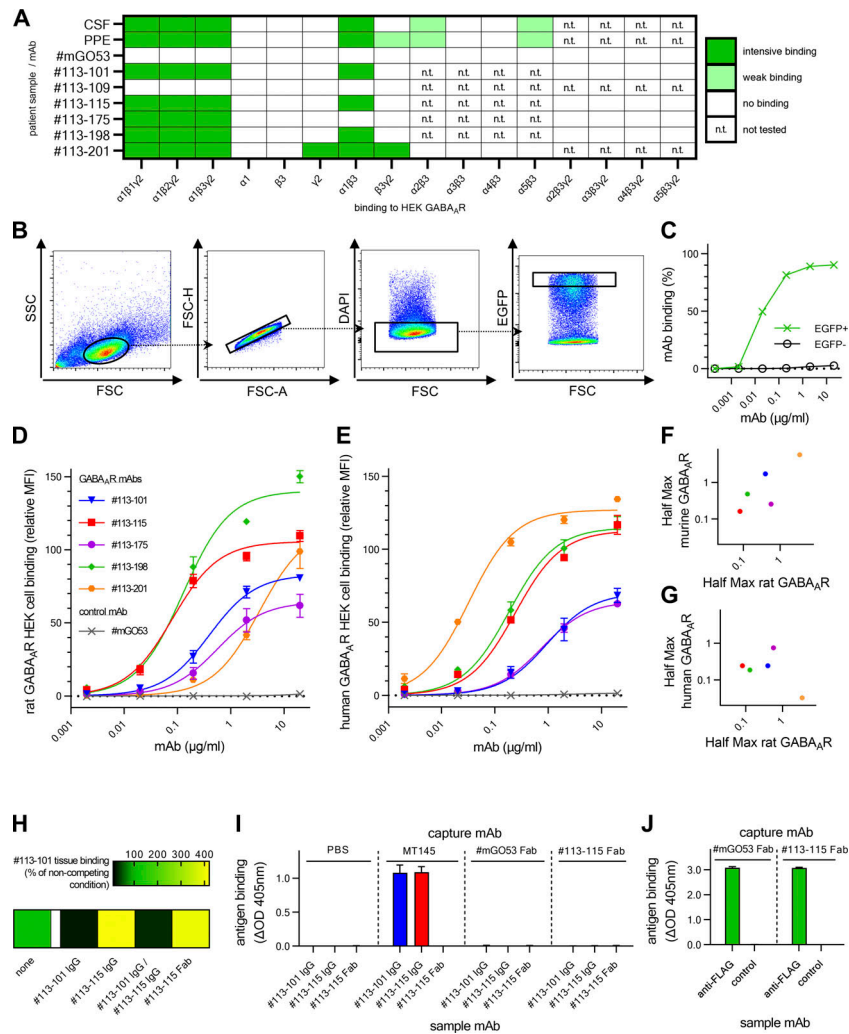


Figure S3. Characterization of GABA_AR mAb binding to native receptors. (A) Overview of binding from patient’s polyclonal samples and derived recombinant GABA_AR mAbs in CBAs using COS7 cells overexpressing individual or multiple GABA_AR subunits as indicated. Examples are shown for $\alpha 1\beta 3\gamma 2$, $\alpha 1\beta 3$, $\beta 3$, and $\gamma 2$ in Fig. 2 A. Patient’s CSF and PPE showed CBA-binding patterns similar to the derived CSF mAbs with prominent $\alpha 1$ reactivity and additional weak binding to COS7 cells expressing $\alpha 2\beta 3$, $\alpha 5\beta 3$ (both), and $\beta 3\gamma 2$ (PPE only). #113-101, #113-115, and #113-198 selectively target $\alpha 1$, as detecting cells expressing $\alpha 1\beta 3$ and $\alpha 1\beta 3\gamma 2$, but not $\beta 3$ or $\gamma 2$ alone (Fig. 2 A). Specificity was confirmed by the absence of reactivity to $\alpha 2\beta 3\gamma 2$, $\alpha 3\beta 3\gamma 2$, $\alpha 4\beta 3\gamma 2$, and $\alpha 5\beta 3\gamma 2$. #113-175 detects GABA_AR only when $\alpha 1$ and $\gamma 2$ are coexpressed, but not in any other combination containing a different α -subunit ($\alpha 2$ – $\alpha 5$) with $\beta 3\gamma 2$ coexpression. mAb #113-201 binds the subunits $\alpha 1$ and $\gamma 2$ independently (Fig. 2 A). The α -subunit-mediated reactivity is specific to $\alpha 1$, as CBA overexpressing different α -subunits ($\alpha 2$ – $\alpha 5$) in combination with $\beta 3$ was not detected. GABA-negative control #mGO53 showed no binding. All GABA_AR-negative mAbs from patient’s CSF repertoire with anti-neuronal reactivity (exemplarily shown for #113-109) and negative control #mGO53 showed no binding. Note that $\beta 3$ alone is expressed on the cell surface, but $\alpha 1$ alone is not (Ebert et al., 1999). (B–C) A flow cytometry approach analyzing HEK cells transfected with rat or human $\alpha 1\beta 3\gamma 2$ GABA_AR and EGFP was used to complement tissue-based quantification of GABA_AR mAb binding to native receptors (Fig. 2 B). (B) Selection of cells for analysis was based on sequential gating on a homogeneous cell population in forward scatter (FSC) and sideward scatter (SSC), single cells, live cells (negative for DAPI), and lastly the population of 30% highest EGFP signal as a marker for transfection. (C) Concentration-dependent GABA_AR mAb #113-115 binding to EGFP-positive and thus GABA_AR HEK cells in comparison to EGFP-negative HEK cells. Similar data were obtained from all GABA_AR mAbs. (D and E) Relative MFI values were used to model binding to HEK-expressed rat GABA_AR (D) or human GABA_AR (E) using nonlinear regression models for one site-specific binding (Table S2). Bars indicate mean \pm SEM from $n = 3$ experiments. (F and G) Regression model-derived Half Max concentrations (50% of saturation binding = MFI_{max}) are compared between the flow cytometry assays using rat or human $\alpha 1\beta 3\gamma 2$ GABA_AR and the murine tissue-binding assay (Fig. 2 A): The correlations indicate generally similar binding between assays ($R = -0.70$, $P = 0.23$ in F; $R = -0.21$, $P = 0.77$ in G), with the exception of #113-201, which bound weakly to murine and rat GABA_AR but was the strongest binder to human GABA_AR. (H) For analysis of competitive binding (in addition to Fig. 2 C), fluorophore-coupled GABA_AR mAb #113-101 was stained on unfixed murine brain tissue in combination with GABA_AR mAbs as full IgG or Fab in excess as indicated. Quantified mean MFIs as relative values to noncompetition conditions are shown as a heat map, each from 30 ROIs from two independent experiments. Receptor binding competition is visualized in black and signal enhancement in yellow. (I) An ELISA assay was used to exclude binding of #113-101 to the variable domain of the #113-115. High-binding plates were coated with commercial anti-human IgG MT145 or Fab fragments of control mAb #mGO53 or GABA_AR mAb #113-115 as indicated in column group titles above. Sample mAbs (human IgG or Fab) were then applied as indicated in column labels below and detected using commercial detection antibody MT78-ALP. Note that MT145 and MT78-ALP are Fc specific; thus, Fabs could not be detected when used as sample mAb. Bars indicate mean \pm SD from triplicates of $n = 2$ experiments. (J) A control ELISA assay was used to confirm successful coating of Fab fragments to high-binding plates. Plates were coated as above before application of commercial mouse anti-FLAG antibody (as sample mAb) for capture by Fab fragments. Bars indicate mean \pm SD from triplicates of $n = 2$ experiments.

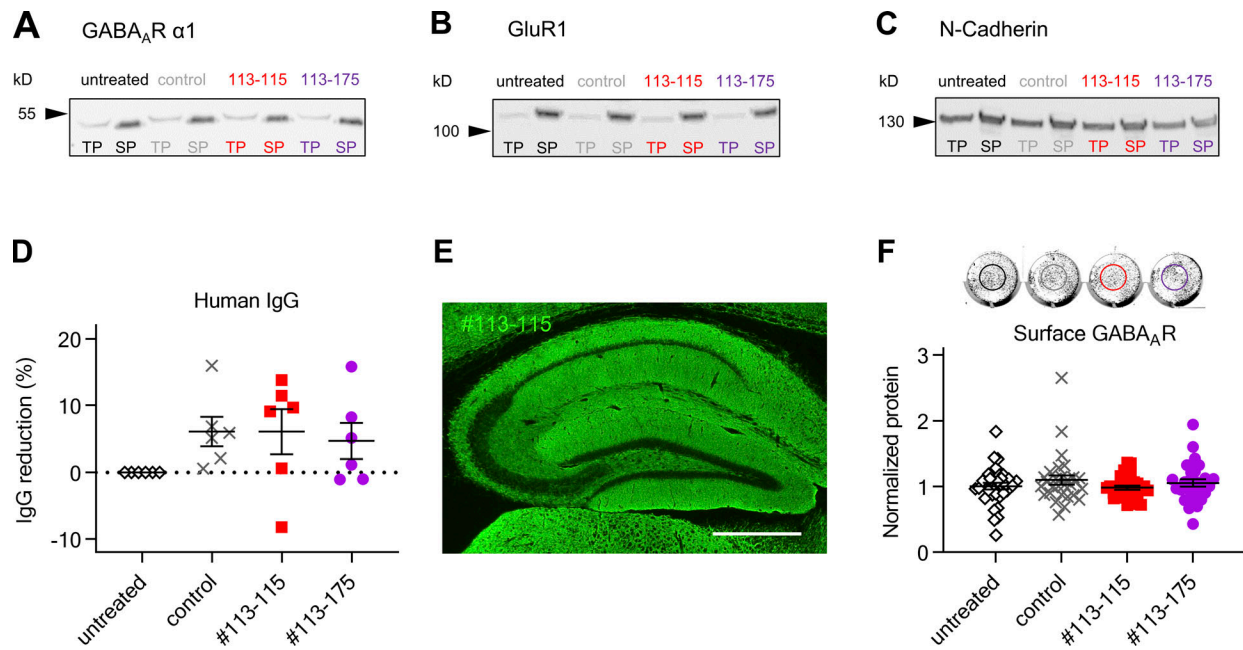


Figure S4. **Quantification of protein expression from cultured neurons treated with GABA_AR mAbs.** (A–C) Representative Western blots of total protein (TP) and biotinylated surface protein (SP) samples from neocortical rat neurons after preincubation with indicated GABA_AR or control mAb #mG053. Blots were stained with commercial antibodies against the α1-subunit of GABA_AR (A), the GluR1-subunit of α-amino-3-hydroxy-5-methyl-4-isoxazolepropionic acid receptors (B), and N-Cadherin (C). Quantifications of protein levels are shown in Fig. 4, G–J. (D) Quantification of human IgG from neocortical rat neuron culture media used for Western blotting experiments (Fig. S4, A–C; and Fig. 3, G–J). The reduction of IgG was measured as the relative difference between post-treatment medium and matched source medium samples, which have not been applied to the culture [relative reduction = (concentration_{source medium} – concentration_{post-treatment medium})/concentration_{source medium}]. Bars indicate mean ± SEM; *n* = 6 experiments from two separate cultures. (E) Representative immunofluorescence staining of post-treatment neuronal culture medium containing mAb #113-115 on an unfixed murine brain section confirmed GABA_AR reactivity of the antibody by typical staining pattern, as shown here in hippocampus. Scale bar indicates 500 μm. (F) Quantifications of GABA_AR surface levels from reader-based immunohistochemistry recordings from neocortical rat neurons after preincubation with indicated human GABA_AR or control mAbs. Representative recording is shown on top from neurons after live staining with a commercial antibody against the α1-subunit of GABA_AR. Quantifications revealed no difference. Bars indicate mean ± SEM; *n* = 6 experiments from three separate cultures.

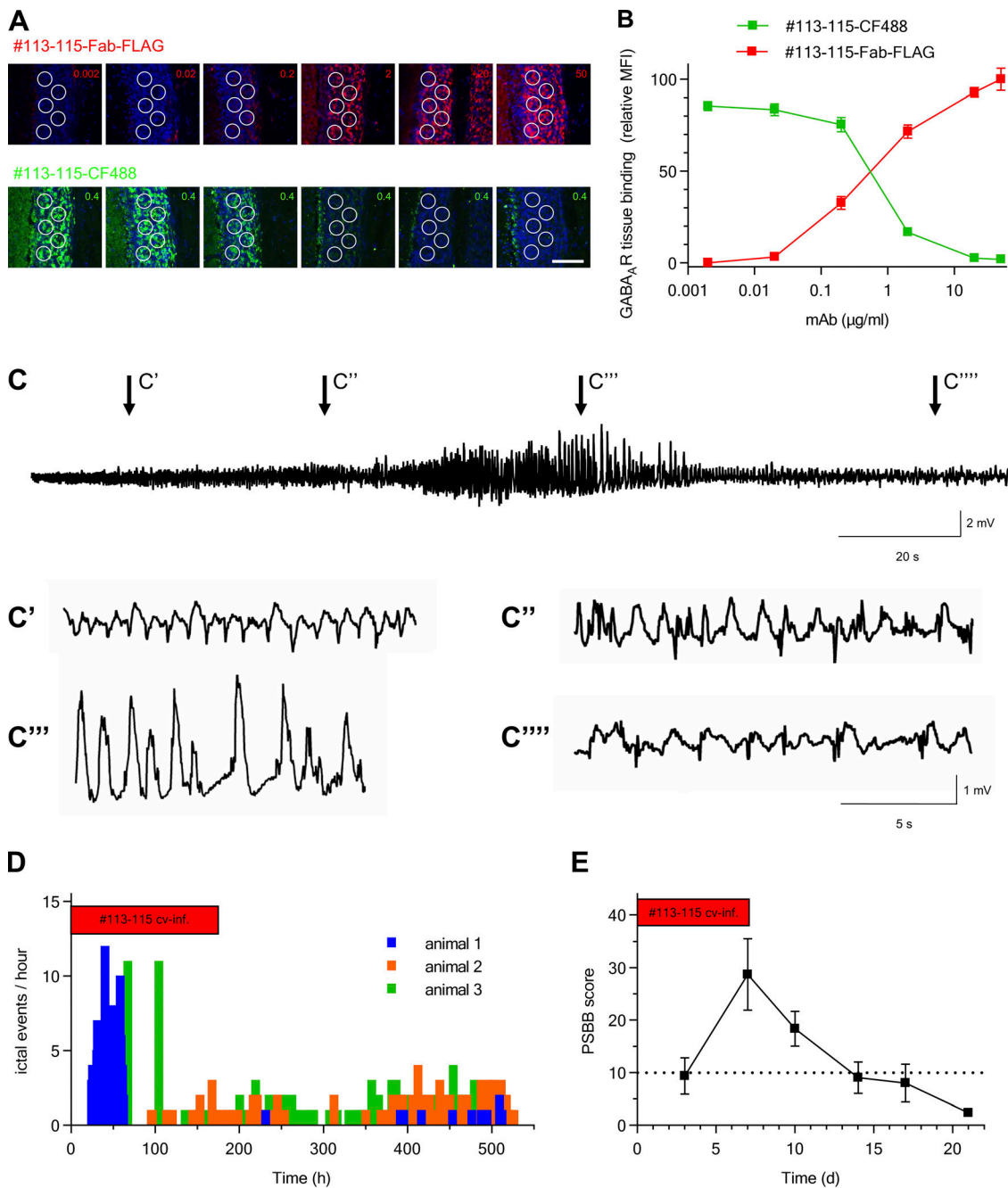


Figure S5. **Competition of mAb #113-115 Fab and #113-115 IgG for binding to murine brain tissue.** (A) To confirm competitive binding to the identical target GABA_AR mAb #113-115 as Fab fragment was stained at serial dilutions as indicated in the presence of fluorophore-coupled #113-115 IgG (#113-115-CF488) at threshold concentration of 0.4 µg/ml (green). Binding of Fab was visualized using an anti-FLAG secondary antibody (red; nuclei in blue). The MFI was measured separately for Fab and IgG binding in identical ROIs within granule cells of the cerebellum. Representative scale bar indicates 100 µm. (B) MFI values from 18 ROIs of *n* = 2 independent experiments are shown as mean ± SEM. (C) Representative EEG recording from GABA_AR mAb-infused rat is shown with an example of a Racine stage 5 seizure with video-EEG and closeups of different EEG patterns during the recorded seizure. The corresponding video is included as [Video 2](#). (D) Distribution of the detected ictal events over time as analyzed with Neuroarchiver seizure detection software in a subgroup of three animals that were recorded for a prolonged period of 21 d and that had received GABA_AR mAb infusion over 7 d (red bar). Data from 7-d recording period for all animals including controls is shown as [Fig. 5 D](#). (E) From the same animals, the post seizure behavioral battery (PSBB) tests were performed and scored for 21 d. The dotted line represents the PSBB score of 10, above which the animals are likely to demonstrate aggression and hyperexcitability on testing, which strongly correlates with the development of spontaneous recurrent seizures. Bars indicate mean ± SEM. cv-inf, cerebroventricular infusion.

Video 1. **Catatonias and epileptic seizures in mice after intrathecal infusion of GABA_AR mAbs.** (A) Control mouse receiving high-dose control IgG showed normal explorative behavior 3 d after intrathecal infusion. (B) In contrast, infusion of high-dose GABA_AR mAb #113-115 led to severe catatonias and focal epileptic seizures after 3 d. (C) Direct comparison of spontaneous behavior in mice receiving either GABA_AR (left) or control mAb #mGO53 (right). (D) In mice receiving lower doses of GABA_AR mAb, catatonias and focal seizures occurred later (day 6) and were less pronounced. (E) Worsening of motor abnormalities at day 10 in animals receiving high-dose GABA_AR mAb with hyperexcitability and increased seizure frequency. (F) In contrast, control mice remained healthy and showed normal explorative behavior after 14 d of intrathecal mAb infusion. conc., concentration; d3, day 3; d4, day 4; HL, heavy λ; HK, heavy κ.

Video 2. **Video recording of Racine stage 5 seizure in a rat after intrathecal infusion of GABA_AR.** Video shows clinical presentation of the seizure corresponding to the EEG recording shown in Fig. S5 C.

Provided online are three tables. Table S1 presents sequence and reactivity data from GABA_AR encephalitis CSF antibody repertoire. It lists Ig sequence features and reactivity characteristics for mAbs with corresponding identifier (mAb ID) isolated from CSF cells of different phenotypes, including ASCs, MBCs, and NMBCs. Table S2 shows regression models for GABA_AR mAb binding to unfixed murine brain. Table S3 characterizes disease symptomatology in GABA_AR encephalitis mouse model.